Atmospheric Environment 333 (2024) 120652

Contents lists available at ScienceDirect

Atmospheric Environment

journal homepage: www.elsevier.com/locate/atmosenv

Towards integration of LOTOS-EUROS high resolution simulations and heterogenous low-cost sensor observations

Ioanna Skoulidou [a,*], Arjo Segers [a], Bas Henzing [a], Jun Zhang [b], Ruben Goudriaan [b], Maria-Elissavet Koukouli [c], Dimitrios Balis [c]

[a] TNO, Air Quality and Emissions Research, Utrecht, the Netherlands
[b] TNO, Environmental Modelling, Sensing and Analysis Group, Petten, the Netherlands
[c] Laboratory of Atmospheric Physics, Aristotle University of Thessaloniki, Greece

HIGHLIGHTS

- Assimilation of particulate matter measurements over Eindhoven area in the Netherlands using low-cost sensors.
- Impoved PM_{10} and $PM_{2.5}$ simulations over Eindhoven using measurements from official and low-cost networks.
- Updated PM emissions estimated from the assimilation experiments are higher than the *a priori* emissions.
- Assimilations of PM suggest changes in temporal profiles of updated emissions.

GRAPHICAL ABSTRACT

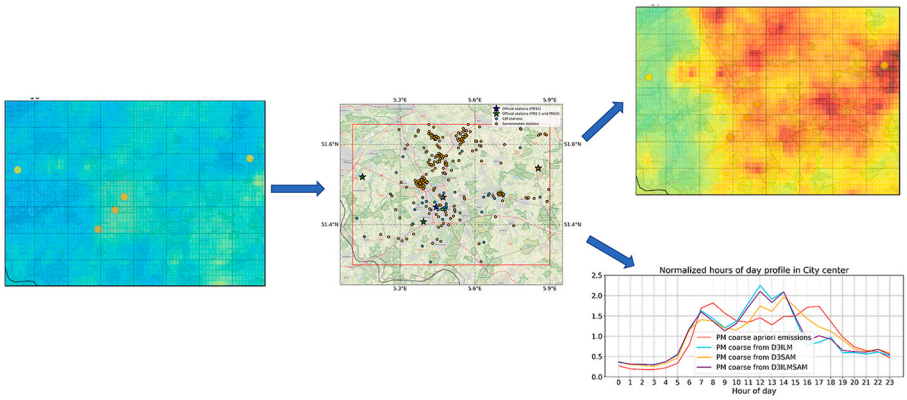

ARTICLE INFO

Keywords:
Data assimilation
Low-cost sensors
LOTOS-EUROS
Particulate matter
Emissions

ABSTRACT

Official air quality monitoring networks are often scarce and unevenly spatially distributed. In recent years, the use of low-cost sensors next to official networks is increasing. These additional networks provide measurements of high spatial and temporal resolution and potentially reveal patterns and emissions sources that are hard to detect with conventional methods. In this work, the data assimilation method implemented around the LOTOS-EUROS chemistry transport model is employed to assimilate measurements from heterogenous low-cost sensor networks around the city of Eindhoven in the Netherlands in November 2021. Three data assimilation experiments are performed and evaluated against a free run of the model. In the first one, measurements from the low-cost Innovatief Lucht Meetsysteem (ILM) network are exploited. In the second one, the citizen science network SamenMeten is used and in the third one, a combination of both datasets is applied. In the assimilation experiments at a domain around the city of Eindhoven, it is shown to be essential to use boundary conditions from an assimilation on a larger domain to account for the variability in pollution that originates from sources outside the domain of interest. Such an improvement in boundary conditions counts for a decrease in the initial free run negative biases of 45% for PM_{10} and 23% for $PM_{2.5}$ in the city of Eindhoven. The assimilation of low-cost

* Corresponding author. TNO, Air Quality and Emissions Research, 3584 CB, Utrecht, the Netherlands.
E-mail address: ioanna.skoulidou@tno.nl (I. Skoulidou).

https://doi.org/10.1016/j.atmosenv.2024.120652
Received 13 December 2023; Received in revised form 24 April 2024; Accepted 8 June 2024
Available online 10 June 2024

measurements in the region after the correction of the boundary conditions decreases the absolute PM_{10} biases in the 3 independent official stations over the city of Eindhoven further from −4.4 μg m^{-3} to about 0.8 μg m^{-3} averaged over the three experiments. Also, the correlation coefficient is increased from 0.75 to 0.89 and the normalized root mean square is decreased from 0.47 to 0.25. We conclude that the improved boundary conditions and assimilation of observations from dense low-cost networks are able to improve the LOTOS-EUROS simulations at urban scale.

1. Introduction

Particulate matter (PM) refers to solid and liquid particles suspended in air and forms one of the major airborne pollutants. It adversely affects the human health as it is made of inhalable particles impacting the respiratory and cardiovascular systems (Kampa and Castanas, 2008). In 2019, 99% of the world's population was living in places where the WHO air quality guidelines levels were not met (WHO, 2021). The impact of PM on human health is associated with the size of the particles, which is mainly defined as $PM_{2.5}$ and PM_{10} for aerodynamic diameters smaller than 2.5 μm and 10 μm respectively. PM also affects the climate due to its impact on the radiance budget of the atmosphere. High PM concentrations contribute to haze pollution (Zhao et al., 2013) and radiative forcing (Forster et al., 2007). The particles originate mainly from combustion (e.g. road traffic and industry), tire and break wear, soil erosion, forest fires and sea salt contributions (Liu et al., 2018). Karagulian et al. (2015) found that globally $PM_{2.5}$ in urban areas originates as 25% from traffic, 15% by industrial activities, 20% by domestic activities, 22% from unspecified anthropogenic pollution sources and 18% from natural dust and sea salt.

Regional chemical transport models (CTM) give the opportunity to understand and study the dynamics of PM and its concentration over urban regions. CTM's play an important role in the implementation of air quality regulations and policy measures (Saikawa et al., 2011; Wang et al., 2015). However, models are sensitive to uncertainties related to parametrizations and input information needed for the simulations. Solazzo et al. (2013) compared PM concentrations simulated with 10 different state-of-the-art regional models in Europe and concluded that in all cases PM_{10} is severely under-predicted by the models, showing mean fractional errors higher than 0.75, due to mainly underestimated anthropogenic and natural emissions as well as errors in the meteorological data. Various studies evaluating PM concentrations from regional models have shown an underestimation in the simulations as well, and suggested that updates in the existing emissions inventories and their temporal resolution are needed (Gašparac et al., 2020; Lopes et al., 2021).

LOTOS-EUROS model has been widely used in studies covering different regions of the globe and forms one of the eleven models that are used in the operational ensemble of Copernicus Atmosphere Monitoring Service (CAMS, https://atmosphere.copernicus.eu/) which provides daily analyses and forecasts over Europe. A data assimilation system based on the Ensemble Kalman Filter (EnKF) technique is used for assimilation of air quality observations. Studies have been already conducted using the data assimilation module around LOTOS-EUROS as well. Curier et al. (2012) assimilated in situ measurements of O_3 over Europe for spring and summer of 2007. The analyzed O_3 in that study showed a significant improvement with the average correlation coefficient for the daily maximum ozone concentration improving from 0.72 to 0.83 and the average Root Mean Square Error (RMSE) reducing from 20.8 to 16.9 μg m^{-3}. Skoulidou et al. (2021) used NO_2 satellite observations from TROPOspheric Monitoring Instrument (TROPOMI) on board the Sentinel-5 Precursor (S5P) satellite with the EnKF assimilation around LOTOS-EUROS, in order to quantify strong declines in NO_x emissions originating from power plants in Greece. The bias in NO_2 between the model and the observations from a station near the biggest power plant in the area decreased from 10.5 μg m^{-3} to 2 μg m^{-3} after the assimilation of the satellite data. Lopez-Restrepo et al. (2020) assimilated PM_{10} and $PM_{2.5}$ measurements from a total of 12 in situ stations in the LOTOS-EUROS model using an Ensemble Kalman Filter (EnKF) technique. The assimilation of measurements leads to improved simulations and more detailed emissions inventories for the region. However, surface measurements from official stations are not always present in a sufficient spatial coverage because of high installation and maintenance costs and assimilation in an urban scale is therefore often not possible.

Low-cost sensors have been widely introduced in recent years as a result of technological advances, offering measurements of various trace gases and aerosols. High-density networks of low-cost sensors provide the potential of improving the temporal and spatial resolution of air quality mapping (Schneider et al., 2017) and provide insights into patterns and emission sources (Popoola et al., 2018). Mijling (2020) constructed high resolution NO_2 maps in the city of Amsterdam by assimilating measurements of the low-cost Urban AirQ campaign (Mijling et al., 2018) together with a few available reference stations. This work revealed more detailed NO_2 patterns in areas which are under sampled by the official network of Amsterdam. The study further concluded that the error of the method depends on the accuracy of the air quality model, the number and the quality of observations as well as the distance of sites to the nearest assimilated observation location, with the local error increasing when observations are available only after distances larger than 2 km. Lopez-Restrepo et al. (2021) assimilated hyper-dense low-cost PM measurements of a network established in Medellín (Colombia) in order to improve the performance of the LOTOS-EUROS model in simulating PM. The assimilated simulations managed to reduce the biases between the model and the measurements in the official stations from a mean fractional bias of −0.65 to almost 0. The combination of low-cost dense networks and numerical simulations through assimilation techniques can therefore provide an efficient monitoring system of air pollution. Such techniques may be of added value for health studies and policy making.

In this study, we take advantage of different dense low-cost sensor networks installed in and around the city of Eindhoven in the Netherlands, in order to improve the $PM_{2.5}$ and PM_{10} simulations of LOTOS-EUROS model. PM observations from a low-cost sensor network and an even denser citizen science network are assimilated with model simulations for the month November 2021. In this period, a sufficient number of low-cost sensors were installed, and concentrations were typically quite high in the region due to (among others) domestic heating. In section 2 the region of Eindhoven together with the distinct sensor networks used in this work are described. Furthermore, the LOTOS-EUROS model that is used in this study and the assimilation method are shortly described, together with the assimilation experiments considered. In Section 3, the impact of improved boundary conditions and the results of the three different assimilations performed are analyzed together with an evaluation of the technique. In section 4 the updated emissions from the assimilation experiments and their temporal profiles are discussed. Finally, in section 5 concluding remarks and further suggestions are provided.

2. Materials and methods

2.1. Region of study

The city of Eindhoven is situated in the south of the Netherlands and

is the fifth largest city in the country with a population density in 2020 of more than 2.670 habitants per km^2 (CBS, 2019). The center of Eindhoven is mainly composed by low-rise commercial and residential buildings (Blocken et al., 2016). The city is characterized by a temperate oceanic climate, affected both by the North Sea and the Atlantic Ocean (Ascenso et al., 2021), with cool summers and moderate winters while the predominant winds are South-West. The region of the study is shown in Fig. 1 with the city of Eindhoven in the center, and also showing the surrounding cities and villages, the major high-ways and roads, and the airport. In the area surrounding Eindhoven a lot of livestock farming is present too, and PM pollution from these activities is an increasing concern of inhabitants in the region.

According to Ascenso et al. (2021) Eindhoven is largely influenced by traffic emissions and probably also by emissions related to household- and office-heating during winter-time. Various industries are located in the city of Eindhoven while in the west side of the city the second largest airport of the Netherlands (Fig. 1) is operating which hosted more than 6.5 million passengers in year 2019 (https://opendata.cbs.nl/#/CBS/en/dataset/37478eng/table). Most polluted areas are also found in the west part of the city. In February, March and November fine mode aerosol is dominant in the region, which could be attributed to emissions from domestic heating. In summer, a larger contribution of coarse mode aerosol is present, which could be attributed to harvesting activities. The study is conducted for November 2021 because a sufficient number of low-cost sensors was installed and the PM concentrations in the area were relatively high.

2.2. LOTOS-EUROS model setup and input data

2.2.1. LOTOS-EUROS simulations

In this study the 3D CTM LOTOS-EUROS (Manders et al., 2017) is used to simulate PM_{10} and $PM_{2.5}$ concentrations in the lower troposphere. The gas-phase chemistry in the model is a modified updated version of CBM-IV (Gery et al., 1989), while for secondary inorganic chemistry ISORROPIA II (Fountoukis and Nenes, 2007) is used. Secondary organic aerosols (SOA) are not considered in this study. Both mineral dust and sea salt emissions are calculated online in the model. Mineral dust emissions in the model can be a result of wind-blown dust, resuspension caused by traffic and agricultural practices and are calculated using meteorology-dependent parameterizations that are further described in details in Schaap et al. (2009). Sea salt emissions are calculated based on wind speed at 10 m and sea surface temperature following Mårtensson et al., 2004 and Monahan et al. (1986). NO emissions from soils are calculated online as well using a parameterization depending on soil type and soil temperature (Novak and Pierce, 1993). Emissions from forest fires are obtained from the Global Fire Assimilation System (GFAS) (Kaiser et al., 2012).

Model simulations were performed in a nested domain configuration as seen in Fig. 2. Three different domains were used in order to achieve a high resolution simulation over the area of Eindhoven. A summarized description of the three domains is shown in Table 1. Domain 1 (in blue color) is the largest domain with the lowest resolution (0.25° × 0.25° longitude × latitude, about 15 km × 25 km at this latitude) covering neighboring urban agglomerations that emit large amount of pollutants, such as Brussels, Dusseldorf, Amsterdam and Rotterdam. The boundary conditions in this domain are obtained by the Copernicus Atmosphere Monitoring Service global Near Real Time product (CAMS NRT, https://atmosphere.copernicus.eu/, last access: 25/11/2021) at a spatial resolution of 35 km × 35 km and a 3 hourly temporal resolution. The first inner domain, called hereafter domain 2 (in green color), was set with a resolution of 0.10° × 0.10° (about 5 km × 10 km) and is configured to use the concentrations from domain 1 as boundary

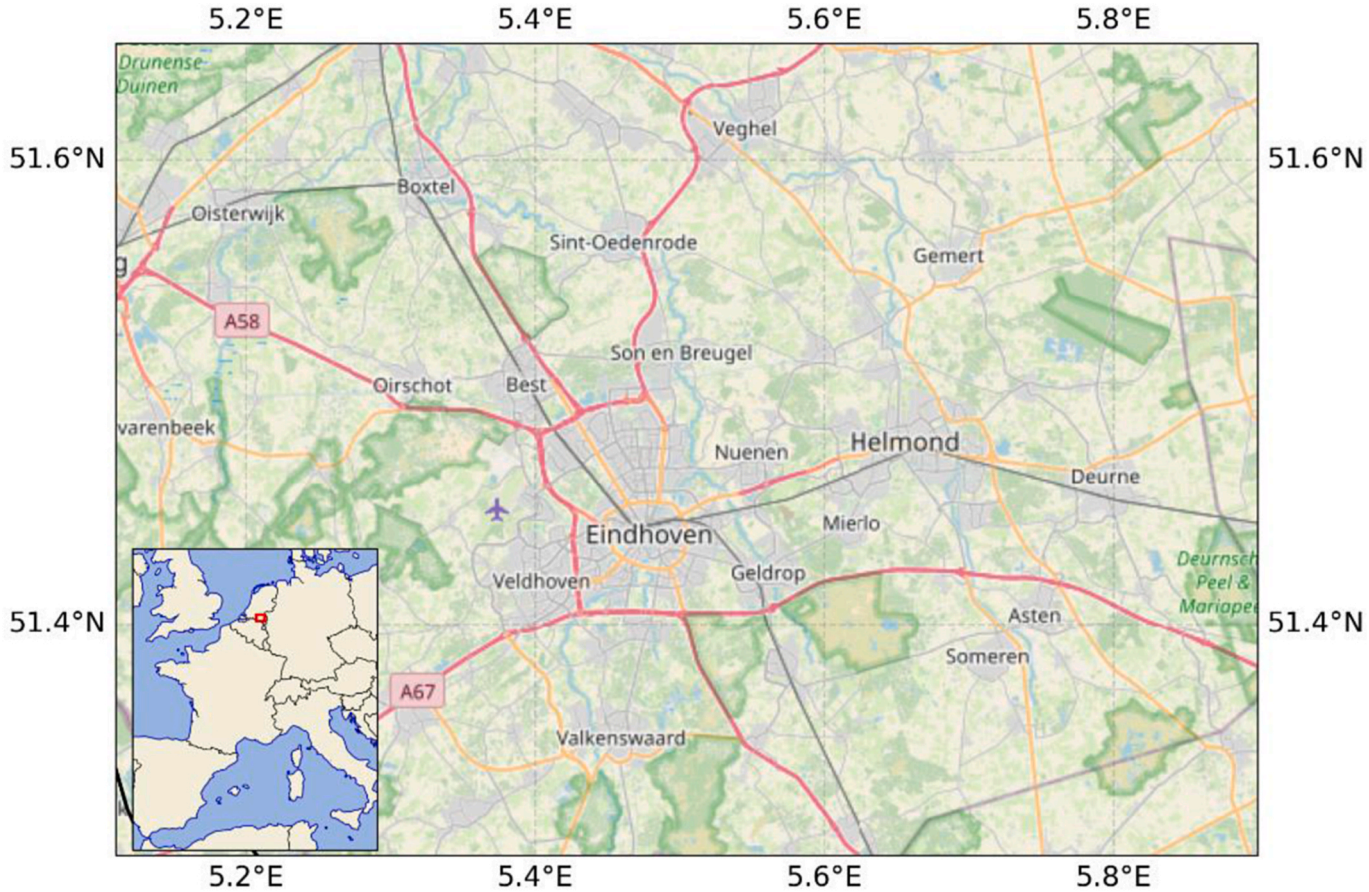

Fig. 1. Map of the main region of interest in this study.

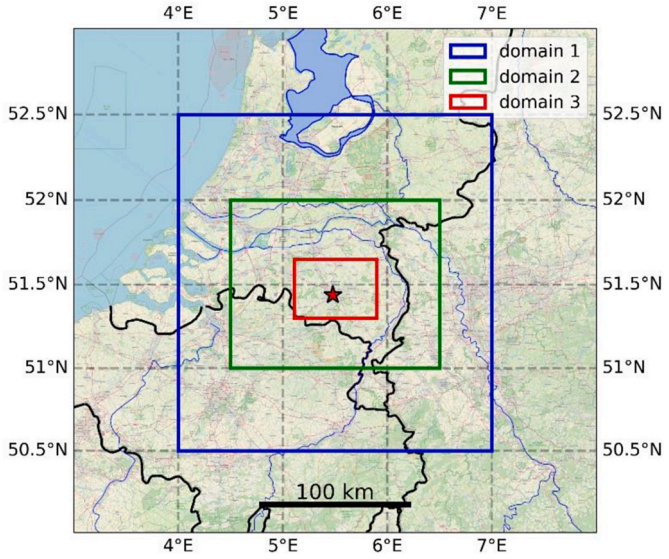

Fig. 2. The threefold nested domains with increasing spatial resolution considered in this work. The city of Eindhoven is depicted with the red star.

Table 1
Description of the three domains.

Domain name	Domain edges	Spatial resolution	Boundary conditions	Emissions
domain 1 – D1	4 °–7° E, 50.5°-52.5° N	0.25° × 0.25°	CAMS-NRT	CAMS-REG
domain 2 – D2	4.5 °–6.5° E, 51°-52.° N	0.10° × 0.10°	D1	CAMS-REG
domain 3 – D3	5.11 °–5.9° E, 51.3°-51.65° N	0.01° × 0.01°	D2	Dutch inventory

conditions. Finally, domain 3 (in red color) is the smallest domain within domain 2 with the finest resolution (0.01° × 0.01°, about 0.5 km × 1 km) and covers the domain of interest for this study and includes the city of Eindhoven and the surrounding municipalities. In each simulation domain the model is driven by meteorological data obtained at 7 km × 7 km horizontal resolution from the Integrated Forecasting System (IFS) of the European Centre for Medium-Range Weather Forecast (ECMWF). Although the resolution of this meteorological data is rather coarse, it provides sufficient information for the chosen domains where elevated orographic elements are hardly present; for future studies, a dedicated higher resolution meteorology should be considered however.

2.2.2. *A priori emissions*

The *a priori* anthropogenic emissions used in domain 1 and domain 2 were taken from the CAMS-Regional European emissions (CAMS REG) database for 2017 (Kuenen et al., 2022) with a spatial resolution of 0.10° × 0.05° (about 5 km × 5 km). Maps of the total PM_{10} and $PM_{2.5}$ emissions in November 2021 are shown in Fig. 3. The emissions used are re-gridded at the horizontal resolution of the two domains. The anthropogenic emissions used in domain 3 were obtained from the country's Emission Register (http://www.emissieregistratie.nl/, last access: 19/11/2021) which provides the annual releases of more than 350 pollutants to air, soil and water in the Netherlands. The emissions are obtained at a horizontal resolution of 0.01° × 0.01° and are valid for the year 2018. This inventory was only used for domain 3 since it is only available for the Dutch domain and does not cover domain 2 and domain 1. Higher spatial resolution emissions were not available for domain 2 and domain 1 and as a results model simulation resolution in these domains was much lower. The aggregated emissions of PM_{10} and $PM_{2.5}$ used as input in the model simulations are also shown in the right panels of Fig. 3. Highest PM_{10} and $PM_{2.5}$ emissions are reported for the city of Eindhoven and in the south of the domain where the industrial area in the north of Valkenswaard municipality is located. Furthermore, high emissions are found east from Eindhoven in the city of Helmond, and to the north in the region of Veghel.

Both emission inventories contain for every sector considered the annual total, which is distributed into hourly values applying profiles for the month-in-the-year, day-of-the-week and hour-of-the-day. The break down of annual to hourly emissions used in this study is based on the default temporal profiles provided with the TNO-MAC-II (TNO-Monitoring Atmospheric Composition and Climate) inventory (Kuenen et al., 2014). The available temporal profiles that accompany the anthropogenic emissions are generally based on statistics and form one of the main sources of uncertainty in the model. The annual emissions of pollutants are distributed in hourly emissions using monthly, weekly, daily and hourly profiles per pollutant sector in order to produce hourly simulations. However, these profiles are mainly based on usual Western European conditions. Therefore more uncertainties may exist over other European countries. Furthermore, they are based on old and probably outdated source of information and as a result they do not take into account sudden changes in human behaviors such us the changes during COVID-19 restrictions (Fioletov et al., 2021) or implementation of new environmental laws (Castellanos and Boersma, 2012).

2.3. *Measurement networks*

2.3.1. *Official network*

Hourly measurements of PM are available from the official air monitoring network via the European Environmental Agency (EEA, https://www.eea.europa.eu/). The locations of the official air quality stations used in this study are shown in Fig. 4 and denoted with blue color if they provide measurements of both PM_{10} and $PM_{2.5}$ and green color if only PM_{10} is measured. Time series from 3 stations in the city of Eindhoven, 6 stations in the surroundings, and 3 stations just over the country border are obtained for November 2021 for the needs of the current study. The official stations located in the center of Eindhoven consist of two urban traffic stations (NL00236 and NL00237) measuring only PM_{10} and one urban background station, NL00247, measuring both PM_{10} and $PM_{2.5}$. Four stations located outside the city and characterized as regional background stations are the NL00131, NL00230, NL00246 and NL00644, while two stations (NL00241 and NL00442) are classified as urban background stations. Furthermore, hourly data of PM_{10} and $PM_{2.5}$ are obtained from 2 stations in Belgium (BETN016 and BELHH08) characterized as rural and urban background respectively and PM_{10} measurements from a rural background station in Germany (DENW066).

Some stations of the official network are used for the assimilation of PM in domain 2 while the rest of them are used to evaluate the results. Only the ones characterized as background stations are used for the improvement of concentrations in domain 2 since they have to be representative for background concentrations and not local contributions. Moreover, stations are chosen in order to be well distributed over the domain. Stations located outside the Netherlands are considered essential for representing transboundary pollution into the country as well as stations located in the Netherlands but close to the edges of domain 2 to represent pollution transported from sources outside of the domain. For this reason three stations in Belgium and Germany (BETN016, BELHH08 and DENW066) as well as stations NL00644 and NL00246 located near the domain edges are used to assimilate PM. Finally, stations NL00230 and NL00131 are selected for the assimilation process since they provide measurements both on $PM_{2.5}$ and PM_{10}, are characterized as background stations and are better distributed in the domain considering the stations that have already been selected for the process. The assimilation stations are denoted with a circle marker in Fig. 4, while the stations in star symbols are used to evaluate the results (validation stations).

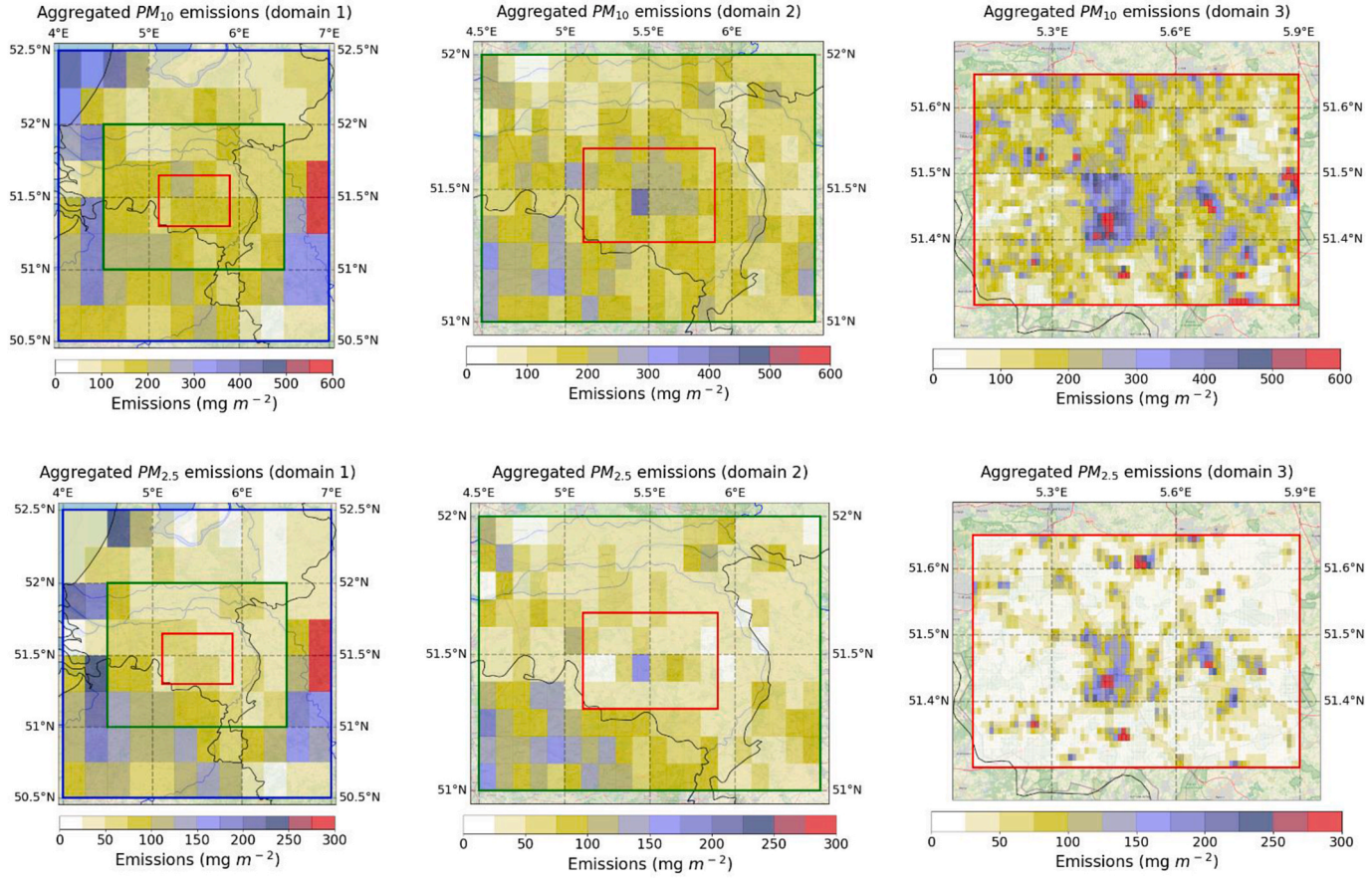

Fig. 3. PM_{10} (top) and $PM_{2.5}$ (bottom) *a priori* emissions summed in November 2021 as used for the domain 1 (left), domain 2 (middle) and domain 3 (right) fine resolution simulations.

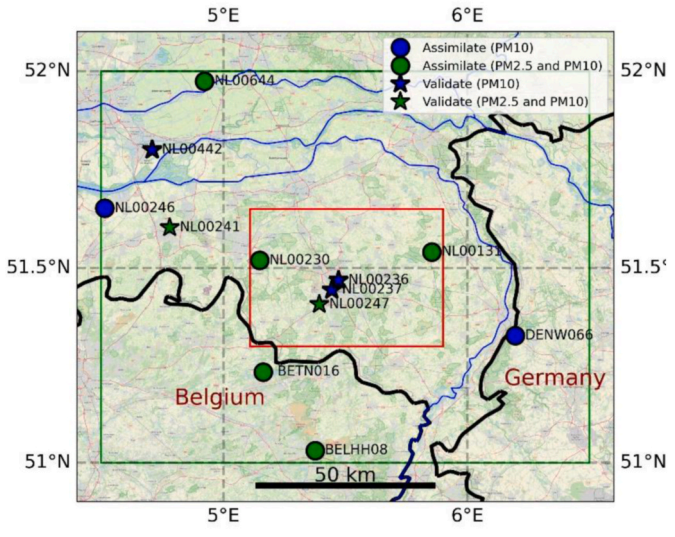

Fig. 4. Stations from the official network used in domain 2, shown in the green rectangle. Domain 3 is delimited by the red rectangle.

2.3.2. ILM low-cost sensors

The low-cost sensors used in this study belong to the urban ILM system (Innovatief Lucht Meetsysteem, English: Innovative Air Measurement System). The sensors are installed in and around the city of Eindhoven under the AiREAS initiative (https://aireas.com/en/, last access: 10/01/2022) as a collaboration of public health authorities, research institutes and university in order to monitor air quality. The basic sensor for PM is the Shinyei PPD42 optical sensor. The sensors have carefully been installed depending on the spatial and temporal variability of the air quality in the region and on local sources (roads, industry, traffic lights, building works, airport and locations that people are exposed) (Hamm et al., 2016).

Measurements of PM_{10} and $PM_{2.5}$ of the ILM network are assimilated in domain 3 and the simulated results are evaluated by the official network, LML stations. For this study, 10 min temporal resolution PM_{10} and $PM_{2.5}$ measurements from 44 ILM airboxes located around the city of Eindhoven were obtained for November 2021 from https://ilm2.site.dustmonitoring.nl (last access, 10/01/2022). The hourly averaged data were calculated. Furthermore, the PM_{10} levels were set equal to $PM_{2.5}$ when the $PM_{2.5}$ levels exceeded the PM_{10} values. This occurs on average 13 times per month based on the 10 min measurements. The mean hourly PM_{10} and $PM_{2.5}$ values over all stations in November together with the standard deviation is given in Fig. 5. The stations spatially cover mostly the city of Eindhoven with some stations located in the surrounding rural areas and Eindhoven airport. The spatial distribution of ILM stations is shown in Fig. 6 (light blue cycles).

2.3.3. Calibration and modification of ILM sensors

The reliability of PM measurements from low cost sensors is many times questionable. Canu et al. (2021) studied in detail the performance of Shinyei PPD42 sensors explaining the difficulty that these sensors have to differentiate a large particle from a set of two or more small particles when the sensors are used without any modification. As a result, they suggest the use of a non-trivial algorithm in order to estimate well the particle concentration. They also conclude that these sensors are not suitable for mobile applications but on the other hand for static

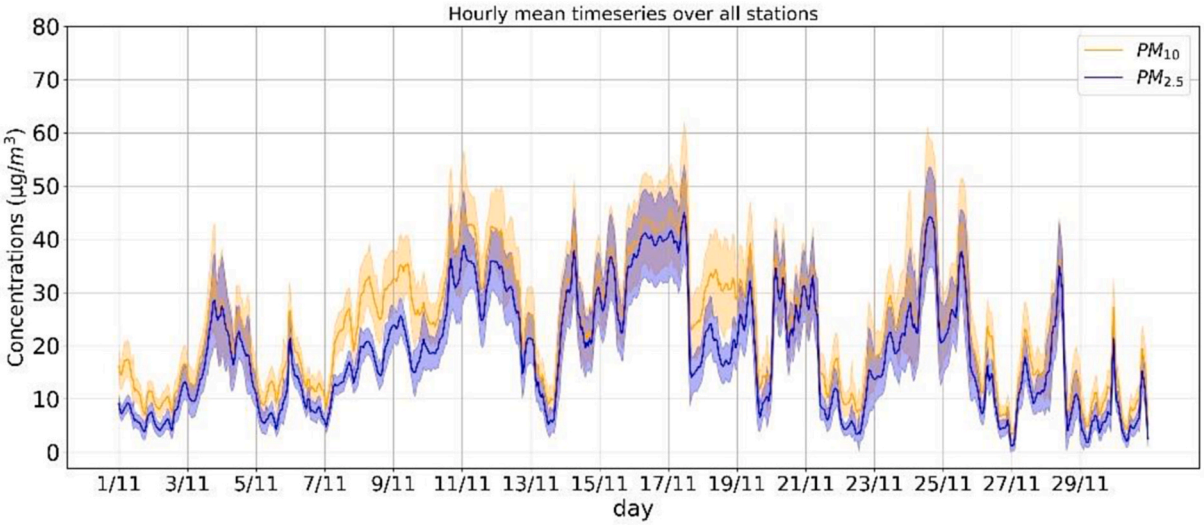

Fig. 5. Hourly mean $PM_{2.5}$ (blue line) and PM_{10} (orange line) over all ILM station in November 2021. The shaded area denotes the standard deviation over all stations over each hour.

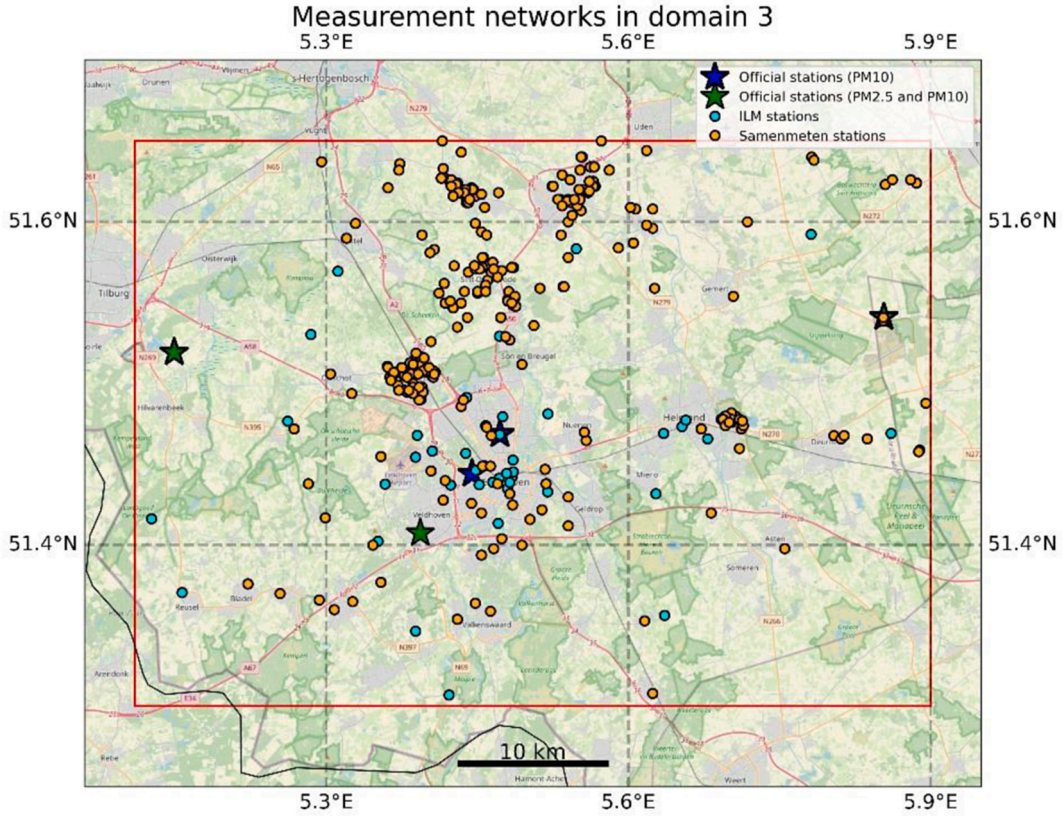

Fig. 6. Locations of the stations of the three different measurement networks in domain 3, depicted in the red rectangle. The official stations are denoted with star symbols in green and blue when they measure both PM_{10} and $PM_{2.5}$ or just PM_{10}, respectively. The ILM stations available for November 2021 are depicted by light blue markers, while the SamenMeten sensors are shown by orange markers.

applications (as they are used in this study), it is possible to reach an acceptable accuracy by integrating the measurements during a long operation time and using a suitable humidity correction.

The commercially available sensors are modified before the setup of the ILM network. The hardware is altered to directly read out the filter's voltage outputs. The generated pulses are related to the particle size because Mie diffusion intensity depends on this. We use this information to deduce the relevant size information to produce independent $PM_{2.5}$ and PM_{10} concentrations by application of different threshold values. Further discussion on the algorithm effectiveness can be found in supplement. In order to calculate the correct concentrations, the calculated mass concentration of the sensors is compared to the Fidas 200 S and the correct calibration factors are determined for the individual particle channels before their installation in the network. The calibration of ILM sensors takes place at a calibration rack in the region of Alkmaar, the Netherlands (Goudriaan et al., 2022). The measurements of each sensor

for a period of at least 2 weeks and assuming sufficient variation in the concentrations are compared with the reference equipment, Fidas 200S, in open air. The calibration is carried out for the different particulate matter fractions. During calibration of the sensors against the reference instrument it was found that both PM_{25} and PM_{10} show high correlations across all boxes. However, it is also found that the deviations of the sensor measurements from reference measurements are magnified at higher values.

The measurements of ILM after their installation are compared with observations from the official network (LML) in order to assess their quality. Furthermore the behavior between ILM stations was examined (Goudriaan et al., 2022). In general, the concentration patterns measured by ILM stations over time were found similar to the LML, with higher absolute differences during wintertime. The measurement network was found suitable for identifying and indicating patterns in particulate matter in time and space at local and regional scale. In particular, comparison between daily LML Genovevalaan PM_{10} (NL10236) and daily ILM station I37 PM_{10} are studied. On average, ILM station measures higher $PM_{10,}$ ~20.9 μg/m^3, than the LML, ~17.2 μg/m^3 for year 2021. The regression slope between ILM and LML measurements is between 1.49 for December and 0.96 for June, while the annual slope is 1.20. The Root Mean Square Deviation (RMSD) is higher in winter than in summer and the annual RMSD is equal to 7.1 μg/m^3. ILM higher deviations during wintertime, when PM concentrations are higher, could also be explained by the results of the calibration; i.e deviations of sensors are magnified at higher values.

As a result, the low-cost sensors observations from the ILM network are considered good enough for the actual scope of this work which is to test and evaluate the added value they can have when we combine them with LOTOS-EUROS model.

2.3.4. SamenMeten citizen science network

SamenMeten (English: Measuring Together) is an innovation citizen science program in the Netherlands launched by the National Institute for Public Health and the Environment (RIVM) in 2016 together with other research institutes, the government, companies and citizens (Rubio-Iglesias et al., 2020). The program was established with a portal (https://samenmeten.rivm.nl, last access: 10/01/2022) as central hub for citizen science and air quality. Citizens can obtain air quality data from this platform but also upload it. Low-cost sensors established by citizens focus mainly on nitrogen dioxide (NO_2) and particulate matter (PM_{10} and $PM_{2.5}$) pollutants. There is a number of uncertainties involved with citizen science low-cost sensors. In particular the measurement errors for particulate matter by the low-cost sensors are highly affected by humidity. Low-cost sensors mainly use optical systems to measure the particles and this leads in interpreting water drops into particles (Wesseling et al., 2019). The RIVM has developed a calibration method to perform corrections concerning the relative humidity of the measurements. The properly calibrated sensors of the network can give an indication of the spatial distribution of the average air quality in an area and the relative variation of concentrations over time. The calibration method continues to evolve, since more robust methods are needed because the data quality is currently not sufficiently high, and more important, the data quality is actually often unknown. Furthermore, the sensor measuring errors can differ between the different types of sensors. In SamenMeten program different types of sensors may be hired by citizens. In addition, the type of location of sensors selected by citizens is not known and any inappropriate use cannot always be identified, for example indoor installation of sensors. The spatial distribution of the SamenMeten network is more irregular than the distribution of ILM sensors and covers mostly the surrounding areas of Eindhoven providing information for the neighboring municipalities of the province. Moreover, the data availability is less reliable, and the time series of some sensors are interrupted or even absent after some moment. The distribution of the sensors is shown by the orange cycles in Fig. 6 together with the locations of the ILM and official stations.

Hourly data from 300 stations located in the study area are obtained from the hub. The calibrated values of PM_{10} and $PM_{2.5}$ are filtered for negative values and for the cases when $PM_{2.5}$ is higher than PM_{10}. This occurs on average 115 ± 82 times in November 2021 based on the hourly measurements for 300 sensors measuring. It should also be mentioned that instruments at some stations record very high values that are not in accordance with the general measurement levels of the official network. For this reason we performed a further data filtering in the data in order to discard the time series that would affect the assimilation results in a deceptive way. As we do not expect the PM concentrations to differ much in a relatively small region as the one in this study, the measurements from the official stations in the region were used to extract information on the PM distribution over the area. According to these, time series of PM_{10} and PM_{25} were rejected when more than 10% of the measurements exceeded the maximum values measured by the official stations, i.e. 180 μg/m^3 and 160 μg/m^3 respectively. Further, time series were rejected when extreme differences between two sequent measurements appeared. The differences between the sequent measurements of the official stations were calculated and the threshold for the values to be excluded was set to 3 times their standard deviation. In particular, when 10% of sequent measurements of PM_{10} was higher than the 50 μg/m^3 (40 μg/m^3 for PM_{25}), the time series were rejected for the assimilation process. Time series of PM_{10} from 26 and of PM_{25} from 21 stations were hence discarded from the study.

It should be mentioned at this point that the goal of this study is not to validate SamenMeten data but to investigate the impact of the citizen science data in the assimilation approach, and the (future) potential of low-cost sensor observations for monitoring particulate matter considering the unknown uncertainties of this data.

2.4. Assimilation experiments

The networks of ILM and SamenMeten sensors that have been introduced in the Eindhoven area monitor the air quality at a resolution that is unprecedentedly high for the region. To explore the potential of these sensor networks for air quality monitoring, we assimilate observations of $PM_{2.5}$ and PM_{10} in high spatial resolution particulate matter simulations performed over the city of Eindhoven and its surroundings. Because of its rather long atmospheric lifetime, particulate matter pollution in the city of Eindhoven is also (highly) affected by pollution originating from the surrounding areas outside domain 3. According to the modelled source specific PM concentrations performed by the TNO Operational Pollution Apportionment Service (TOPAS, https://topas.tno.nl), during November 2021 a large amount of PM_{10} near Eindhoven finds its origin in the wider region containing large urbanized or industrialized areas in the Netherlands and other countries such as Belgium, Germany, France and sometimes even from Poland and Great Britain. Also, sea salt can reach the city. Because of incoming pollution from outside the region, the configuration of assimilation experiments in this study includes also an assimilation of particulate matter measured by official stations in the Netherlands and in the neighboring regions of Belgium and Germany outside of domain 3.

For convenience the different experimental runs are named after their domain and whether assimilation of a specific measurement network took place. Following the nesting configuration used in our study and presented in section 2.2.1, experiments are performed along two different lines in order to gradually move from the low resolution domain 1 simulations ("D1free") to the high resolution domain 3 (D3), as seen in the flow chart presented in Fig. 7 and described in Table 2. In the first type of experiments, the "D2free" simulation on Domain 2 uses the simulations from "D1free" as boundary conditions and subsequently, "D3free" uses the "D2free" simulations as boundary conditions. In the second type of experiments, the "D2OF" simulation at domain 2 uses "D1free" simulations as boundary conditions, and assimilates observations of official stations ("OF") in its domain in order to provide improved simulations and thus improved boundary conditions for D3.

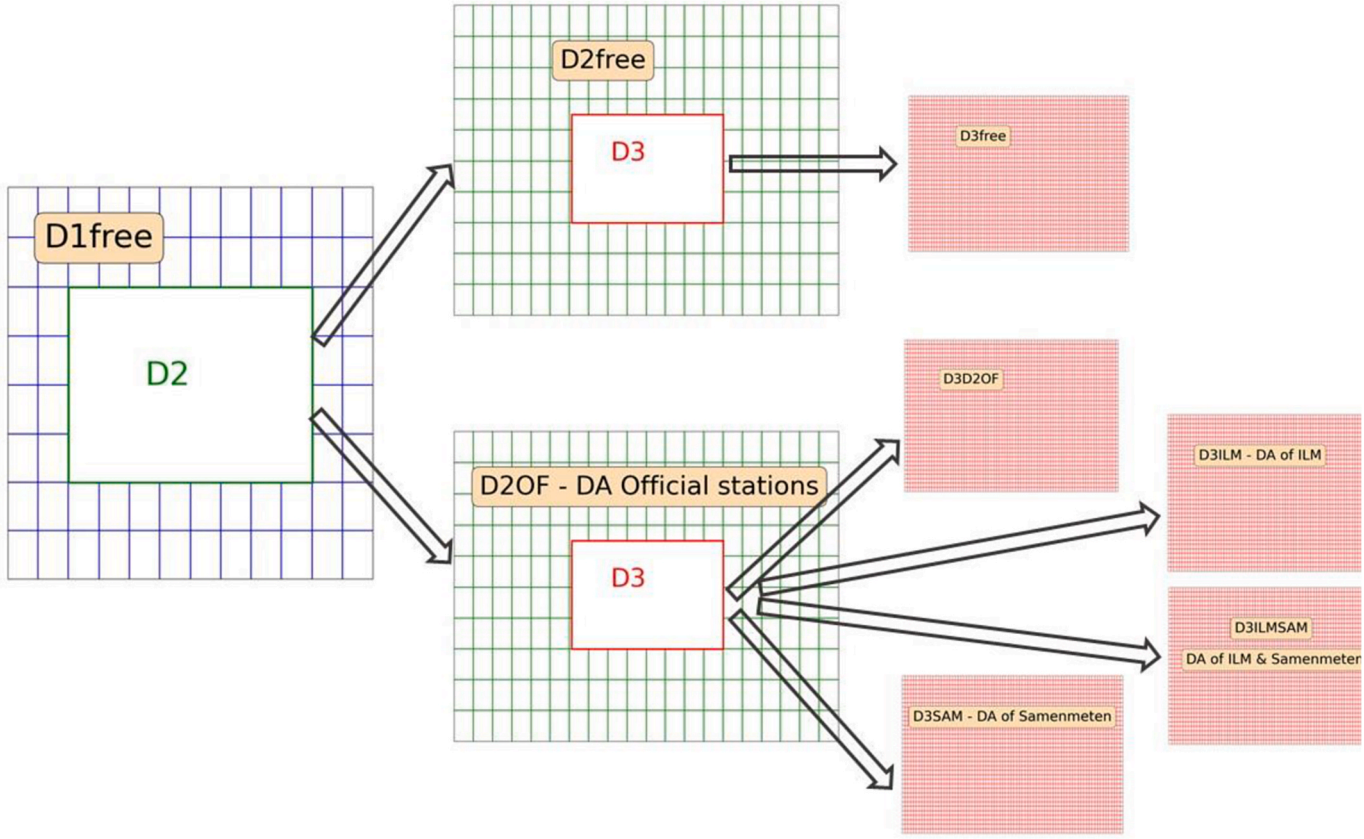

Fig. 7. Flow chart of the steps and the experiments performed in this study. The different domains (D1, D2 and D3) and their spatial resolution is denoted.

Table 2
The description of the model simulations and assimilation experimental runs.

Experiment	Assimilation datasets	Domain	Boundary conditions
Model simulations			
D1free	No assimilation	D1	CAMS
D2free	No assimilation	D2	D1free
D3free	No assimilation	D3	D2free
D3D2OF	No assimilation	D3	D2OF
Assimilated runs			
D2OF	Official network	D2	D1free
D3ILM	ILM	D3	D2OF
D3SAM	SamenMeten	D3	D2OF
D3ILMSAM	ILM and SamenMeten	D3	D2OF

Then, four experimental runs are assumed for domain 3 depending on whether assimilation of measurements is performed and what type of low-cost sensors are assimilated each time. In the first experiment ("D3D2OF"), the improved boundary conditions from "D2OF" are used, while no assimilation of measurements takes place. Then, 3 experiments in domain 3 are performed that assimilate $PM_{2.5}$ and PM_{10} observations from either ILM, or SamenMeten, or from both networks (named as "D3ILM", "D3SAM" and "D3ILMSAM" respectively).

In the case of "D2OF" assimilation, which takes place over domain 2 and is further used to provide improved boundary conditions in domain 3 runs, both boundary conditions and emissions are considered uncertain. On the other hand, in the experimental assimilation runs over domain 3 (i.e. "D3ILM", "D3SAM" and "D3ILMSAM") only local emissions are considered as uncertain parameters since the boundary conditions used in this case are already corrected in "D2OF".

2.5. Assimilation technique and configuration

The assimilation technique used in this study is based on a Local Ensemble Transform Kalman Filter (LETKF) that is implemented around the LOTOS-EUROS CTM, following the implementation by Shin et al. (2016) and already described in Skoulidou et al. (2021). The main goal of EnKF is to estimate an optimal state (analysis) by combining model simulations and observations while taking into account their respective uncertainties. Uncertainties in model simulations could be defined for any parameter in the model or input data used that is partly responsible for the deviations between the forecast and the true state, for example *a priori* emissions, boundary conditions, meteorology, and chemistry. The observation simulation uncertainties may originate from different sources such as instrumental errors, retrieval errors and representation errors. In this study, emissions and boundary conditions are considered as the uncertain model parameters. The uncertain parameters are multiplied by randomly perturbed correction factors which are defined as a colored noise in order to maintain a temporal correlation with the uncertainties and have over a long time window mean of 1 and standard deviation of σ. This temporal length scale, τ, is used to describe variations of the uncertain parameters in time.

The LETKF analysis updates the ensemble per grid cell. For each cell, the available observations at time k are collected within a user specified area surrounding the model grid cell, and these will be used to update the forecast ensemble into an analysis ensemble for this grid cell. Selecting only observations nearby the grid cell is part of the localization procedure which is essential to avoid spurious correlations between elements of the state due to the use of a finite ensemble. These spurious correlations can cause observations to randomly affect the analysis in distant locations (Hunt et al., 2007). For the localization procedure in this case a spatial length scale, ρ, is introduced. The weight of the collected measurements in the analysis decays exponentially from one to

zero as their distance from the analysis grid pixel increases. When a small ρ is chosen the analysis is changing only the grid cells located close to the observations, while if ρ is larger more observations are used for the analysis of the grid cell. Only observations within a distance of 3.5ρ from a grid cell are selected and a Gaussian function is used as the weighting function of the observation localization, given by:

$$f = \exp\left(-0.5\left(\frac{d}{\rho}\right)^2\right) \quad (1)$$

where d is the Euclidean distance between the respective grid pixel to be analyzed and each observation's location.

The optimal configuration of the assimilation experiments was found by performing distinct assimilation tests for the period January 10–15 2021 (while the actual period of interest is November 2021). The goal was to choose the optimal values for the assimilation parameters ρ (spatial scale), τ (temporal scale) and σ (standard deviation of the noise distribution attributed to the correction factors). To achieve this, assimilation results using different values for these parameters were evaluated against the official validation stations, whose data was not included in the assimilation. To evaluate these sensitivity tests and choose the optimal values, statistical parameters have been examined and in particular the correlation coefficient, the bias and the NRMSE. The configuration that suggests better statistics and assimilated simulations closer to the measurements was chosen. The optimal values chosen are shown in Table 3.

For the "D2OF" experiment, the most suitable value for the length scale ρ was found to be 35 km, and for the temporal scale τ a value of 1 day was found. The standard deviation for the relative uncertain parameters σ was set to 50%. The runs in domain 3 are performed on a much higher resolution representative for a more local scale, and hence the optimal configuration for the case of "D3ILM" was also investigated using multiple assimilation experiments. The optimal ρ (length scale) was found to be 3 km and the temporal length τ was in this case as well equal to 1 day. The standard deviation σ was found equal to 500% in this case. This means that the correction factors were permitted to increase the emissions with a factor 5 or more in order to let the model decrease the large discrepancies between the simulations and observations due to the high PM underestimation. Very large and unrealistic corrections to the emissions would be derived in this way, while the underestimation of PM observations should also be attributed to model uncertainties other than the uncertainties in the *a priori* emissions, e.g. missing secondary organic aerosol formation from precursor gaseous emissions, limited chemistry, and incorrect meteorology. For example, Timmermans et al. (2022) suggested that to obtain the total contribution in PM concentrations from combustion processes in LOTOS-EUROS the secondary organic aerosols need to be implemented. Further, Hama et al. (2022) studied the characteristics of PM_{10}-associated organic and elemental carbon over 5 cities in North Europe and found that annual secondary organic carbon contribution to total organic carbon is very significant (more than 50%) with the highest concentrations observed during spring and summer and lowest during winter. This emphasizes further the significance of secondary organic aerosol and its possible impact in the underestimated PM simulation. For this reason a maximum threshold of 5 times the *a priori* emissions was set and larger changes are not allowed. The optimal configuration found for "D3ILM" was also used for the domain 3 assimilations of SamenMeten network ("D3SAM" experiment) and when both ILM and SamenMeten networks were assimilated ("D3ILMSAM" experiment) considering that we focus on very local scales and over the same area.

Table 3
Optimal values chosen for the assimilation scenarios.

Name of run	ρ (km)	τ (days)	σ
D2OF	35	1	0.5
D3ILM, D3SAM, D3ILMSAM	3	1	5

In this study the background and local contributions within domain 3 are corrected with a two step approach. The first step includes the assimilation of the LML measurements representative of background areas in domain 2 and the subsequent use of the assimilated simulations as boundary conditions in domain 3. The second step includes the assimilation of the low-cost sensors representative of local contributions in high resolution simulations within domain 3. Low cost sensors in domain 3 measure PM close to local emissions (roads, households, agricultural areas). This is considered in the assimilation process by selecting a small length scale for the assimilation of low-cost sensors in domain 3 and excluding in this way sources from longer distance. Future developments will focus on different ways to approach this problem in one step. This can include the use of a distinct length scale for each station depending on their type (i.e. urban, traffic, background). In this way, stations considered as background will affect pixels in a larger radius around the measurement location compared to traffic stations during the assimilation process. In this approach the localization length scale, ρ, should be defined by the correlations between measurements and simulations as function of their distance. Similarly the standard deviation, σ, for the background and local uncertainties will be defined separately in one each step.

2.6. Evaluation of the experiments

Simulations from free and assimilated runs are compared to observations of ground based stations of the official network (LML) to evaluate their performance. The metrics used are the absolute (b) and relative biases (rb), correlation coefficients (r) and normalized root mean square error (NRMSE).

The absolute bias investigates the differences between the model simulations, either assimilated or not (SIM), and the observations (OBS) and is calculated according to:

$$b = \frac{\sum (SIM - OBS)}{N} \quad (2)$$

The relative bias (rb) is useful to evaluate the differences in biases between different concentration levels and was calculated according to:

$$rb = \frac{\sum (SIM - OBS)}{\sum OBS} \times 100 \quad (3)$$

The correlation coefficients (r) indicates how strong the relationship between SIM and OBS is and is given by:

$$r = \frac{\sum (SIM - \overline{SIM})(OBS - \overline{OBS})}{\sqrt{\sum (SIM - \overline{SIM})^2 \sum (OBS - \overline{OBS})^2}} \quad (4)$$

where $\overline{SIM}$ and $\overline{OBS}$ are the mean values of the simulations and observations respectively.

Finally Root Mean Square (RMSE) reveals how close are the differences between simulations and observations and the Normalized RMSE (NRMSE) facilitates the comparison between different concentration scales.

$$NRMSE = \frac{RMSE}{\overline{OBS}} \quad (5)$$

where:

$$RMSE = \sqrt{\frac{\sum (SIM - OBS)^2}{N}} \quad (6)$$

3. Results

In these sections the results of all different experiments in domain 2 and domain 3 are presented. The evaluation of the "D2free" and "D2OF"

runs against official stations in domain 2 and the importance of improved boundary conditions are shown. Then, the different assimilation experiments using low-cost sensors are evaluated and compared to the free model run in the domain 3.

3.1. Improved boundary conditions

The mean concentrations of $PM_{2.5}$ and PM_{10} in domain 2 generated from the model free run ("D2free") and the assimilation run ("D2OF") in November 2021 are shown in Fig. 8. The monthly mean measured values used for the assimilation "D2OF" are shown in the circles, while the mean monthly measurements from validation stations are shown in triangles. Both PM_{10} and $PM_{2.5}$ are increased throughout the domain after the assimilation. The largest changes are found in the south, over the Belgium area, and over the city of Eindhoven. A strong increase in the $PM_{2.5}$ concentrations is also observed in the north of the domain.

In order to evaluate the "D2free" and "D2OF" simulations we compare them with daily averaged values over the validation stations. Fig. 9 shows the time series of the daily average PM_{10} concentrations and standard deviation over the 5 available validation stations together with similar values of the "D2free" and "D2OF" runs taken from the corresponding model pixels. The "D2free" run underestimates PM_{10} during the whole period, except for November 24 where the free run simulations are higher than the measurements (and also the "D2OF" simulations). The assimilated concentrations in the "D2OF" run are strongly increased and approach the measurements. For November 16 the averaged assimilated concentrations are actually about 50% higher than the observations; the shaded area shows that the variability in the assimilated simulations is quite high during that day.

The statistics for $PM_{2.5}$ and PM_{10} in November 2021 are summarized in Table 4. For the "D2free" and "D2OF" runs, the simulated concentrations for the grid cells containing the observation sites are averaged for the comparisons (average simulation). The simulations of "D2free" consistently underestimate the measurements by −40% compared to the PM_{10} measurements from the validation stations. After assimilation, the average biases in PM_{10} concentrations are strongly decreased to about −10% when comparing "D2OF" simulations with the measurements. The average correlation coefficient between the measurements and the simulations increases from 0.61 to 0.78 after the assimilation and the NRMSE decreases from 0.55 to 0.37. Similar results are found in the case of $PM_{2.5}$ for which 2 validation stations are available. The $PM_{2.5}$ simulations of "D2free" highly underestimate the measurements in the stations by about −50%; after assimilation, these biases are decreased to about −30% for "D2OF". The correlation coefficients also increased from 0.68 to 0.83 after the assimilation of the measurements and the NRMSE decreased from 0.68 to 0.44.

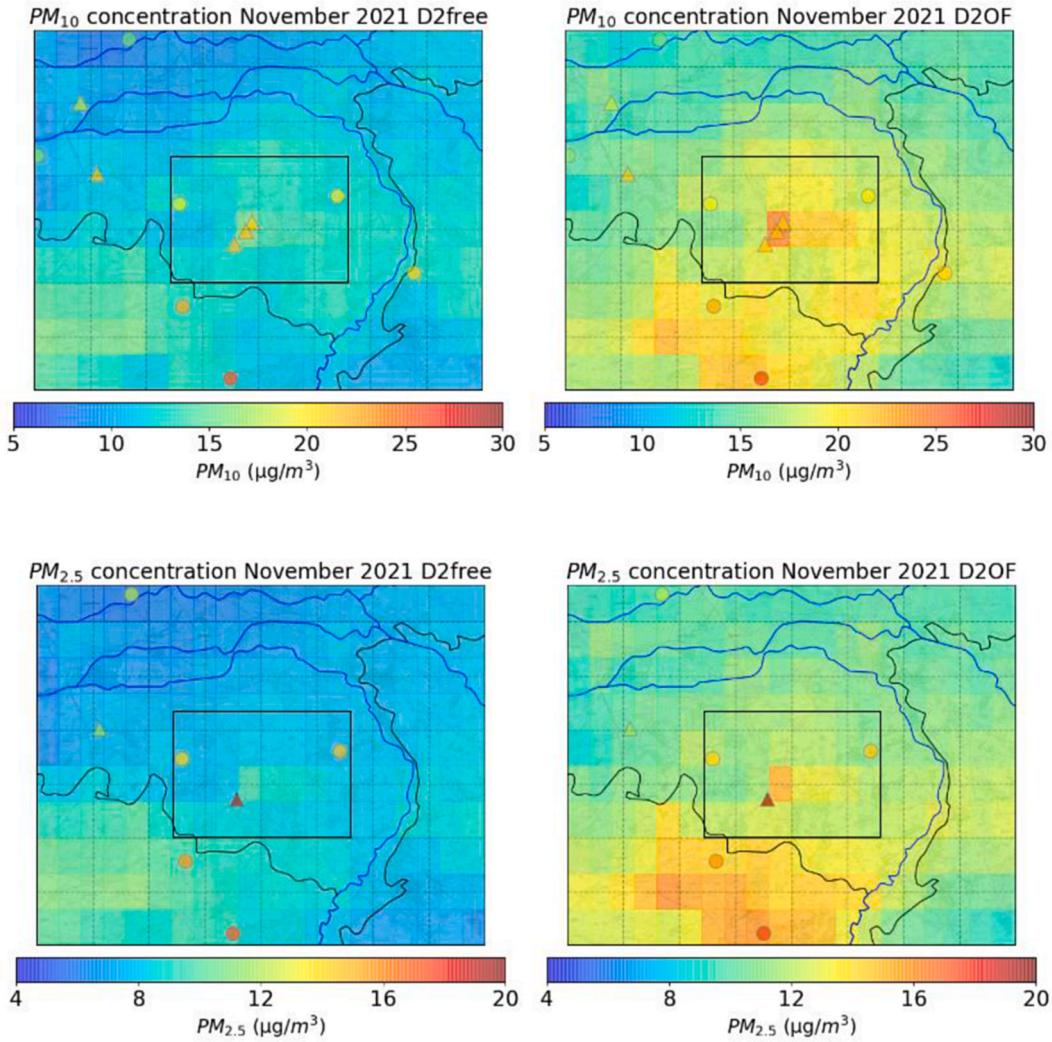

Fig. 8. Monthly mean PM_{10} (top) and $PM_{2.5}$ (bottom) concentrations in domain 2 before (left) and after (right) assimilation. The stations used for the assimilation are denoted with circles, and the validation stations with triangles. The colors of the markers denote the mean values of PM measured by the in situ stations for the same month as the simulations. The black rectangle denotes domain 3.

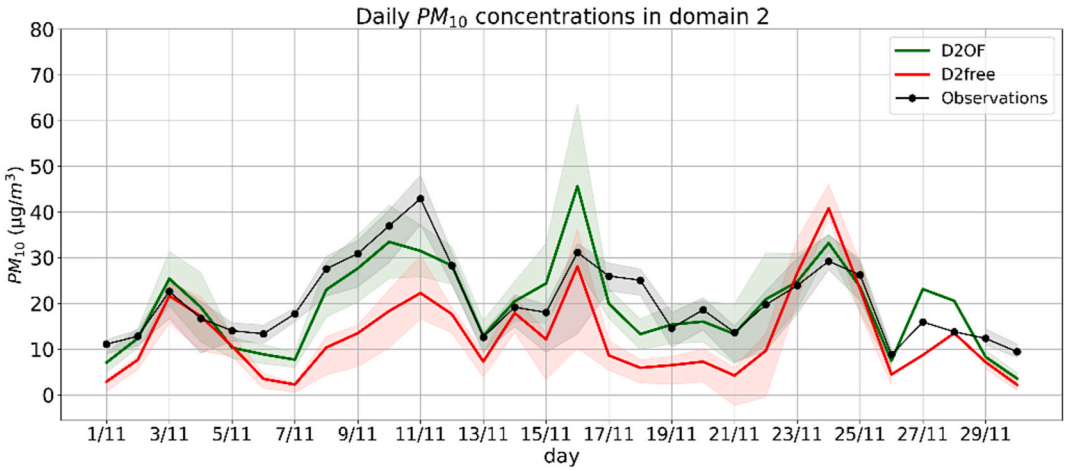

Fig. 9. Mean daily PM_{10} time series of the D2free and D2OF experiments and the average values of observation in the 5 validation stations. The shaded areas stand for the standard deviation of the distribution of mean daily values of the available stations or model pixels.

Table 4
Statistics of the non-assimilation (D2free) run and assimilation of the official stations (D2OF) run compared to the mean $PM_{2.5}$ and PM_{10} observations over the 5 validation stations.

	PM type	PM_{10}	$PM_{2.5}$
Average [µg/m^3]	Observations	20.68	15.16
	D2free	12.76	7.47
	D2OF	19.11	10.55
Corr. Coeff. [-]	D2free	0.61	0.68
	D2OF	0.78	0.83
Bias (µg.m^{-3} [%])	D2free	−7.93 (−39%)	−7.69 (−48%)
	D2OF	−1.58 (−8%)	−4.61 (−27%)
NRMSE	D2free	0.55	0.68
	D2OF	0.37	0.44

The results for "D2OF" show an improvement of the simulations in domain 2 compared to the free run "D2free" simulations. It should be noted here that the whole city of Eindhoven is represented by only one model pixel in this case, hence fine scale urban variations cannot be represented by the model in this experiment. Instead, the "D2OF" simulations are used as lateral boundary conditions in the high resolution runs in domain 3 where dense low-cost networks are assimilated at a resolution that is more suitable for the urban scale.

3.2. Improvement of high resolution PM simulations

The average monthly concentrations from the 5 different experiments performed in domain 3 are shown in Fig. 10 for $PM_{2.5}$ (left) and PM_{10} (right). In the same plots the average monthly measurements from the validation stations in the region are shown in circles using the same color scale. The "D3free" simulations without assimilation (first row) tend to strongly underestimate both PM_{10} and $PM_{2.5}$ over the entire region during the month of interest when compared to the official stations. The high underestimation of both $PM_{2.5}$ and PM_{10} is partly removed when the improved boundary conditions are used in the "D3D2OF" simulation (Fig. 10, second row). However, the mean simulations remain low compared to the mean observations in the center of Eindhoven. When assimilating the ILM measurements, in the "D3ILM" experiment (third row) higher concentrations are obtained in and around the city of Eindhoven for both $PM_{2.5}$ and PM_{10}. However, since there are no ILM observation sites in the west of domain 3 concentrations remain unchanged near the west. Note that the concentrations are higher in the western part of the domain compared to "D3free" experiment due to the improved lateral conditions used in this run, already seen in "D3D2OF" results, which illustrates that the improved boundary conditions are indeed important. In the fourth row, the mean monthly simulations after the assimilation of SamenMeten observations are shown ("D3SAM"). The irregular spatial distribution of the SamenMeten sensors is depicted in the assimilated results together with the lack of measurements in the western part of the domain. Regions such as Best and Helmond, situated north and east of Eindhoven respectively, host many sensors, and increased particulate matter concentrations are simulated. Opposite to this, the west part of the domain shows no important changes due to the scarcity of sensors there. The assimilated concentrations in the eastern part of the domain show extreme high PM_{10} concentrations. It is possible that extreme and unrealistic measurements of PM_{10} from the SamenMeten network result in abnormally high simulations, since the data are not evaluated and only a first order filtering of the stations has been applied in this study. In the last row, the ILM and SamenMeten networks are used together in the assimilation process this time ("D3ILMSAM"). Increased concentrations of particulate matter are shown in the center of Eindhoven as well as in more rural areas such as in Veghel and Sint-Oedenrode in the north of the domain, as visible in the "D3SAM" results. If in addition also the ILM stations are included in the assimilation too ("D3ILMSAM") the extreme values that are found in "D3SAM" experiment are lowered, such as in the area of Helmond located east of Eindhoven.

To obtain a more detailed insight in the performance of the different experiments, the daily average time series at the grid cell where the official station NL00237 is measuring PM_{10} in the center of Eindhoven is given in Fig. 11. The results of the 5 different experiments are shown by lines of distinct colors, and the measurements are given by the black lines. The time series show a high underestimation of PM_{10} throughout the month in the "D3free" model simulation (red line), while this underestimation is decreased when improved boundary conditions are taken into account in "D3D2OF" (green line). The "D3ILM" experiment is represented by the light blue color and follows the measurements quite well, showing increased PM_{10} throughout the period. Similar to "D3ILM", the "D3SAM" experiment (orange line) shows higher concentrations that are closer to the observations in many cases. Between 14 and 17 of November the assimilated experiments overestimate the measurements, while the "D3free" run is actually closer to the measurements. In this period the ILM sensors throughout the city of Eindhoven measure much higher PM concentrations than the official stations. This is illustrated in Fig. 12 where the 2 ILM sensors, #08 and #30, that are located less than 1 km away from station NL00237, are plotted together. As already discussed in section 2.3.3 ILM sensors might positively deviate from LML sensors during wintertime. The "D3ILMSAM" experiment assimilating both ILM and SamenMeten data show quite similar behavior as the "D3ILM" and "D3SAM" runs assimilating

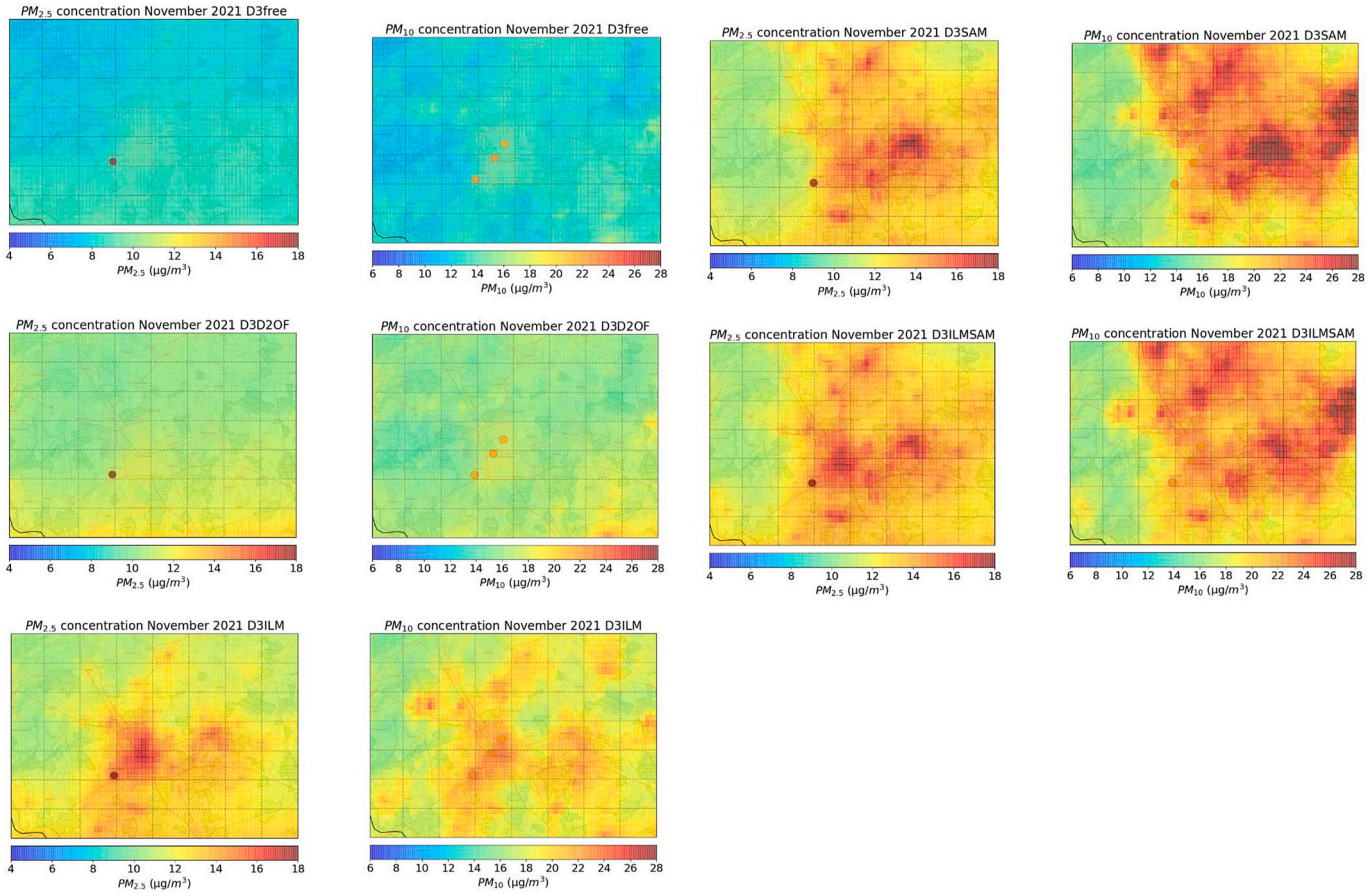

Fig. 10. Mean PM_{25} (left) and PM_{10} (right) surface simulations of the 5 different experiments in domain 3 for November 2021. Starting from top to the bottom the experiments shown are: "D3free", "D3D2OF", "D3ILM", "D3SAM" and "D3ILMSAM". The monthly average value of the validation stations from the official network are denoted with circles and use the same color scale.

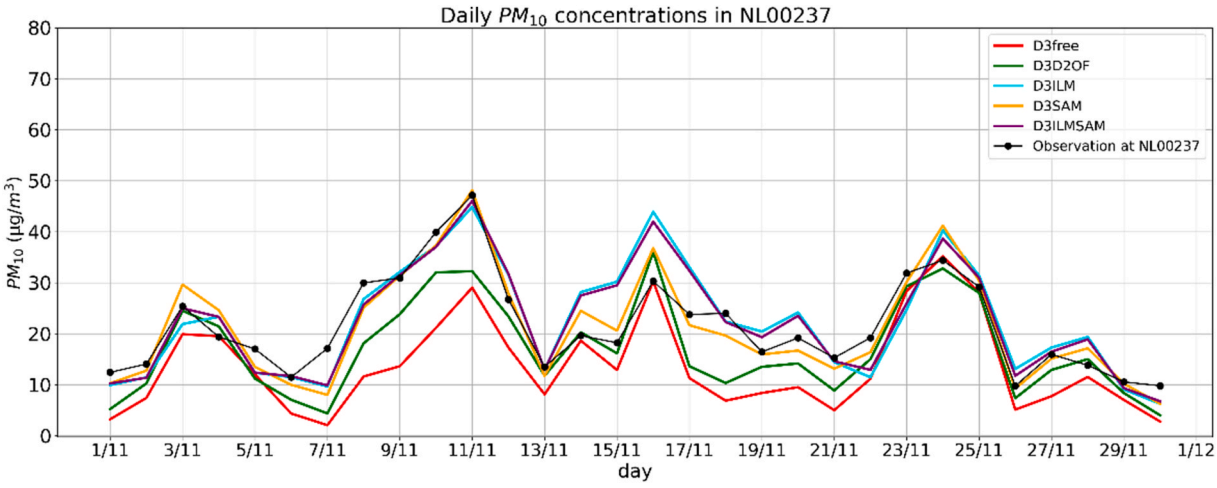

Fig. 11. Time series of mean measured daily PM_{10} concentrations for official station NL10237 and the corresponding simulations of the different experimental runs in the same grid pixel.

just one of the networks, with increase PM_{10} concentrations compared to the free model simulations. Only at November 3 and 27, the "D3ILM-SAM" experiment shows better agreement ith the official station than the "D3SAM" and "D3ILM" experiments.

The statistical results of the 5 different experimental scenarios are summarized in Fig. 13 using relative bias in percent (rb), correlation coefficient (r) and normalized root mean square error (NRMSE) of the daily values as well as in Table 5 in terms of absolute bias (b), correlation coefficient (r) and normalized root mean square error (NRMSE) of the daily values. Most changes are found around the city of Eindhoven because of the availability of low-cost sensors, while simulations near the edges of the domain are mostly changed due to the improved boundary conditions and not the assimilation of low-cost sensors. However this is not the case for the northeast of the domain and for the

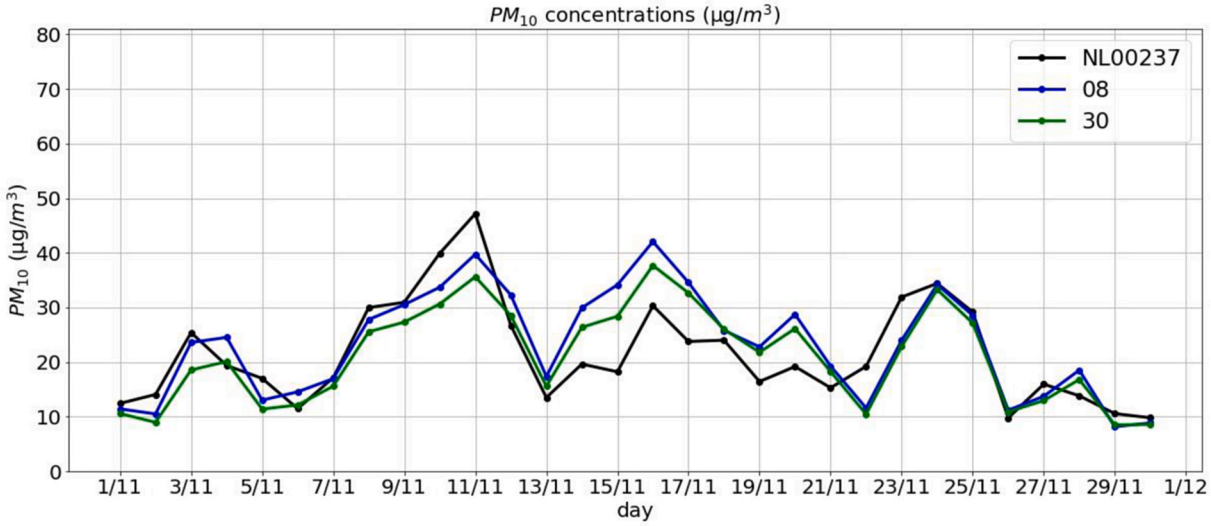

Fig. 12. Time series of mean measured daily PM_{10} concentrations for official station NL00237 and two closest ILM stations #08 and #30.

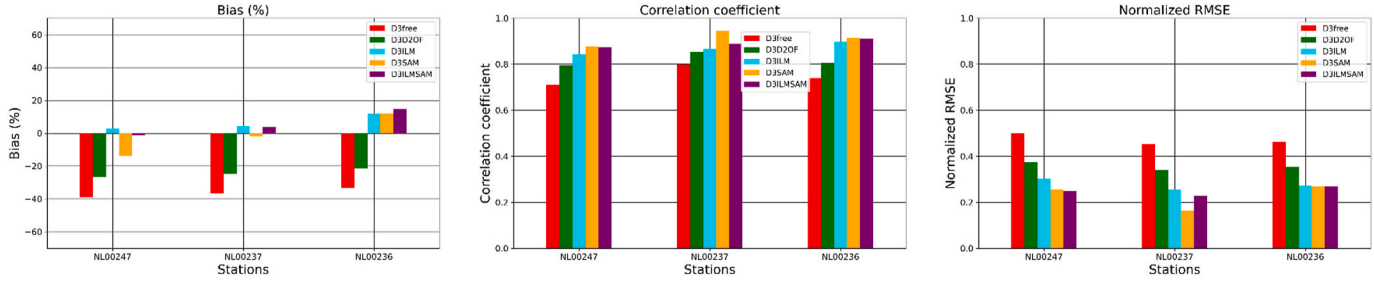

Fig. 13. The relative biases (left), correlation coefficient (middle) and NRMSE (right) of PM_{10} measurements from the official network and the free run and assimilation runs.

Table 5
Statistics (correlation coefficient, biases, NRMSE) for the PM_{10} and $PM_{2.5}$ concentrations between the observations in Eindhoven and the free and assimilated runs.

PM type		PM10			PM2.5
Station		NL 00247	NL 00237	NL 00236	NL 00247
Corr. coef.	D3free	0.71	0.80	0.74	0.82
	D3D2OF	0.83	0.87	0.83	0.90
	D3ILM	0.84	0.87	0.90	0.85
	D3SAM	0.88	0.95	0.91	0.89
	D3ILMSAM	0.87	0.89	0.91	0.86
Bias (µg.m^{-3})	D3free	−8.34	−7.91	−6.91	−10.64
	D3D2OF	−4.86	−4.51	−3.67	−8.20
	D3ILM	0.59	0.96	2.50	−5.12
	D3SAM	−2.93	−0.37	2.53	−6.77
	D3ILMSAM	−0.26	0.84	3.03	−5.14
NRMSE	D3free	0.50	0.45	0.46	0.62
	D3D2OF	0.33	0.30	0.32	0.48
	D3ILM	0.30	0.26	0.27	0.37
	D3SAM	0.26	0.16	0.27	0.41
	D3ILMSAM	0.25	0.23	0.27	0.36

experiments in which SamenMeten network sensors are taking into account in the assimilation (i.e. D3SAM and D3ILMSAM). In these cases, changes in PM concentrations are observed due to the availability of SamenMeten sensors in this regions. The "D3free" simulation highly underestimate the PM_{10} and $PM_{2.5}$ measurements in every stations in the region by an average of around −36% and −56% respectively. The relative biases remain negative when using improved boundary conditions ("D3D2OF") but decrease to −20% for PM_{10} and -43% for $PM_{2.5}$. The relative changes in biases over the stations between "D3D2OF" and "D3free" are about −46% for PM_{10}, suggesting that about 45% of the negative bias in "D3free" is originating by sources outside the domain and removed when using the improved boundary conditions. The relative decrease in $PM_{2.5}$ bias in "D3D2OF" run compared to "D3free" run in the station located near the center of Eindhoven is lower than in PM_{10} and is about −23%.

The biases in PM_{10} between the reference stations and the "D3ILM" are strongly reduced by the assimilation. The biases found between the simulations and the measurements for the three stations in Eindhoven are very small and positive and on average about 6%, suggesting that the bias that has not been removed when using corrected boundary conditions is removed due to the correction of the local emissions in domain 3. The average correlation coefficient and root mean squared are also slightly improved by the assimilation of ILM data (r = 0.87 and NRMSE = 0.28 compared to r = 0.75 and NRMSE = 0.47) in the city of Eindhoven. For $PM_{2.5}$ there is only one official station measuring near Eindhoven showing a decreased bias, with rb = −27% compared to rb = −56% for the "D3free". The relative decrease in the bias of "D3ILM" compared to "D3free" is about 50%, including both corrections due to boundary conditions and emissions. In the "D3SAM" experiment, PM_{10} simulations are improved over Eindhoven with relative biases of −14%, −2%, and 12% for stations NL00247, NL00237, and NL00236 respectively, and a high mean correlation coefficient of 0.91. Similar results are found for the "D3ILMSAM" experiment assimilating both networks, with average relative biases of −1%, 4% and 15% for NL00247, NL00237 and NL00236 respectively and a mean correlation coefficient

of 0.89. The NRMSE decreases even more in "D3SAM" and "D3ILMSAM" and reaches 0.23 and 0.25 respectively. It should be mentioned that in all three experiments the measurements in station NL00236 are slightly overestimated (between 2.5 and 3.0 μg m^{-3}), which could be partly explained for the experiments using ILM sensors since as already shown in Fig. 12, ILM sensors in the center of Eindhoven measure higher PM_{10} than official stations between 13 and 21 of November. Also the "D3ILM" assimilation slightly overestimates measurements of PM_{10} in all 3 stations in Eindhoven, which can be partly explained by the higher values that the ILM network observed in the period between 14 and 17 of November.

4. Updated emissions

In the assimilation experiments, the emissions that contribute to the formation of PM or that are directly emitted as PM, are considered as the uncertain parameters. The emissions of primary PM (i.e. elemental carbon (EC), primary organic matter (POM), dust, and remaining unspecified primary particulate matter (PPM)) as well as emissions that are precursors of secondary inorganic aerosols (i.e. nitrogen oxides (NO_x), ammonia (NH_3) and sulphur oxides (SO_x)) are perturbed in the ensemble using emission correction factors in the assimilation process. It should be noted here that we refer to PM fine (i.e. $PM_{2.5}$) and PM coarse (i.e. PM_{10} – $PM_{2.5}$) and not directly to $PM_{2.5}$ and PM_{10} in order to avoid considering $PM_{2.5}$ twice as an uncertain parameter.

In Fig. 14 the sum of the PM fine and coarse emissions over the month November are shown as present in the prior emissions used for the model runs, and as used in during the assimilation of the different low-cost sensor observations. All assimilation experiments increase the emissions in order to compensate for the underestimation of PM observations. For the city of Eindhoven, a larger increase in PM fine than PM coarse emission fraction is estimated. Furthermore, PM coarse is found to increase more in the surrounding areas than over the city center. These results suggest that the model needs much higher emissions in particular areas in order to compensate for the large discrepancies between measurements and simulations of PM. However, such large increase on the emissions might not be realistic and could point to additional uncertainties in the model that are not taken into account, such as deposition schemes, chemistry, meteorology and the need of including secondary organic aerosol in the model simulations.

The sum of the emissions over domain 3 per component (PM fine, PM coarse, NO_x, NH_3, and SO_x) are shown in Fig. 15. In the "D3ILM" assimilation, the emissions of all 5 components are increased compared to the *a priori* emissions; the increase is even stronger for the "D3SAM" and "D3ILMSAM" experiments. In all experiments, PM fine is increased more than PM coarse; PM fine is 160%, 180% and 210% higher than the *a priori* PM fine emissions for the "D3ILM", "D3SAM" and "D3ILMSAM" experiments respectively, while PM coarse is increased with 100%, 120% and 140% for the same experiments. We should note here, that NH_3 emissions are very low during this period since important sources of NH_3 are in Europe most prominent in spring due to agricultural processes (Paulot et al., 2014; Viatte et al., 2020).

An estimation on the uncertainties of the main pollution sector categories is available from the EMEP/EEA Guidebook (EEA, 2019), and has been adapted to the Gridded Nomenclature For Reporting (GNFR) categories used for CAMS-REG emission inventory by Kuenen et al. (2022). The uncertainty range for PM emissions from road transport, industrial sources and power plants range is estimated to be 50–200%, while for other stationary combustion uncertainties of 100–300% are possible. For agricultural emissions no uncertainty estimate is available because these emission estimates strongly depend on meteorological conditions and assumptions on agricultural practices. The relative importance of different source categories during the month of interest is illustrated in Fig. 16 by time series derived from the TOPAS source apportionment service around the LOTOS-EUROS model (https://topas.tno.nl/). The time series shows in November 2021 for the center of Eindhoven the sectors residential combustion, road transport, industry, energy, and agriculture contribute most to PM_{10} and $PM_{2.5}$ concentrations. The change in the emissions compared to the *a priori*, as mentioned before, range between 100% and 210%, and are in the range of the reported uncertainties. However, we do not believe that the consistent emission update that is suggested by the assimilation, is a realistic indication of the error in the *a priori* emission estimates, as already discussed before the large emission changes found could point to additional uncertainties in the model (i.e. deposition schemes, chemistry and meteorology). Further, the necessary increase in PM emissions (i.e.

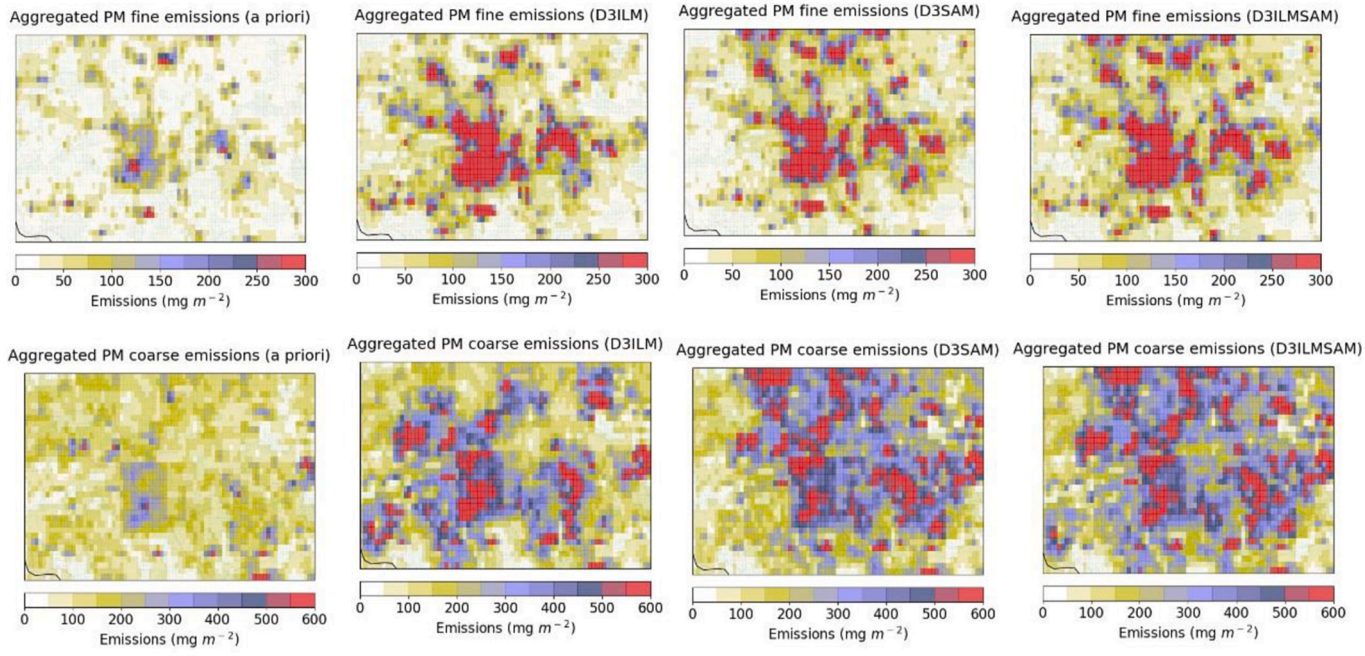

Fig. 14. PM fine (top) and PM coarse (bottom) emissions summed over the month of November 2021 in domain 3 derived from the *a priori* inventory (first column), and the "D3ILM" (second column), the "D3SAM" (third column) and "D3ILMSAM" (fourth column) assimilations.

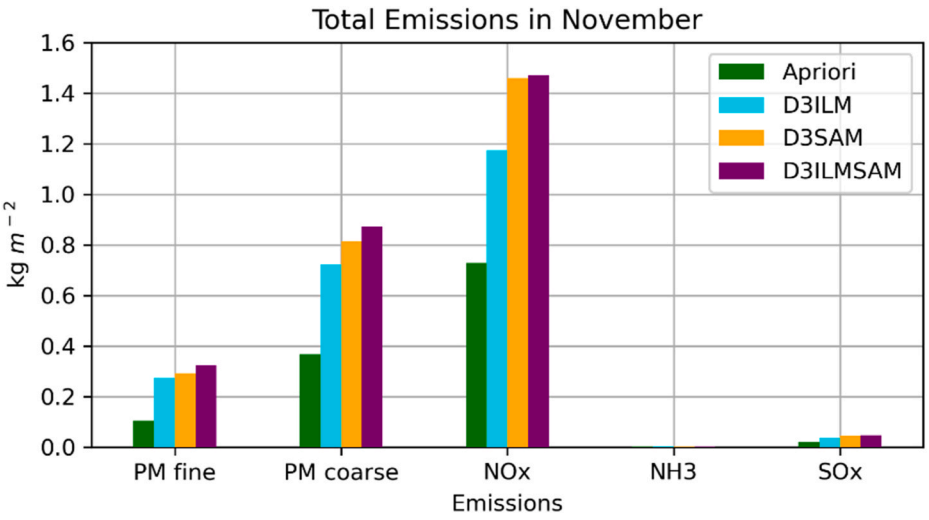

Fig. 15. Sum of emissions in November 2021 over domain 3 from the *a priori* inventory (in green), the D3ILM (in cyan), the D3SAM (in orange) and D3ILMSAM (in purple) experiments.

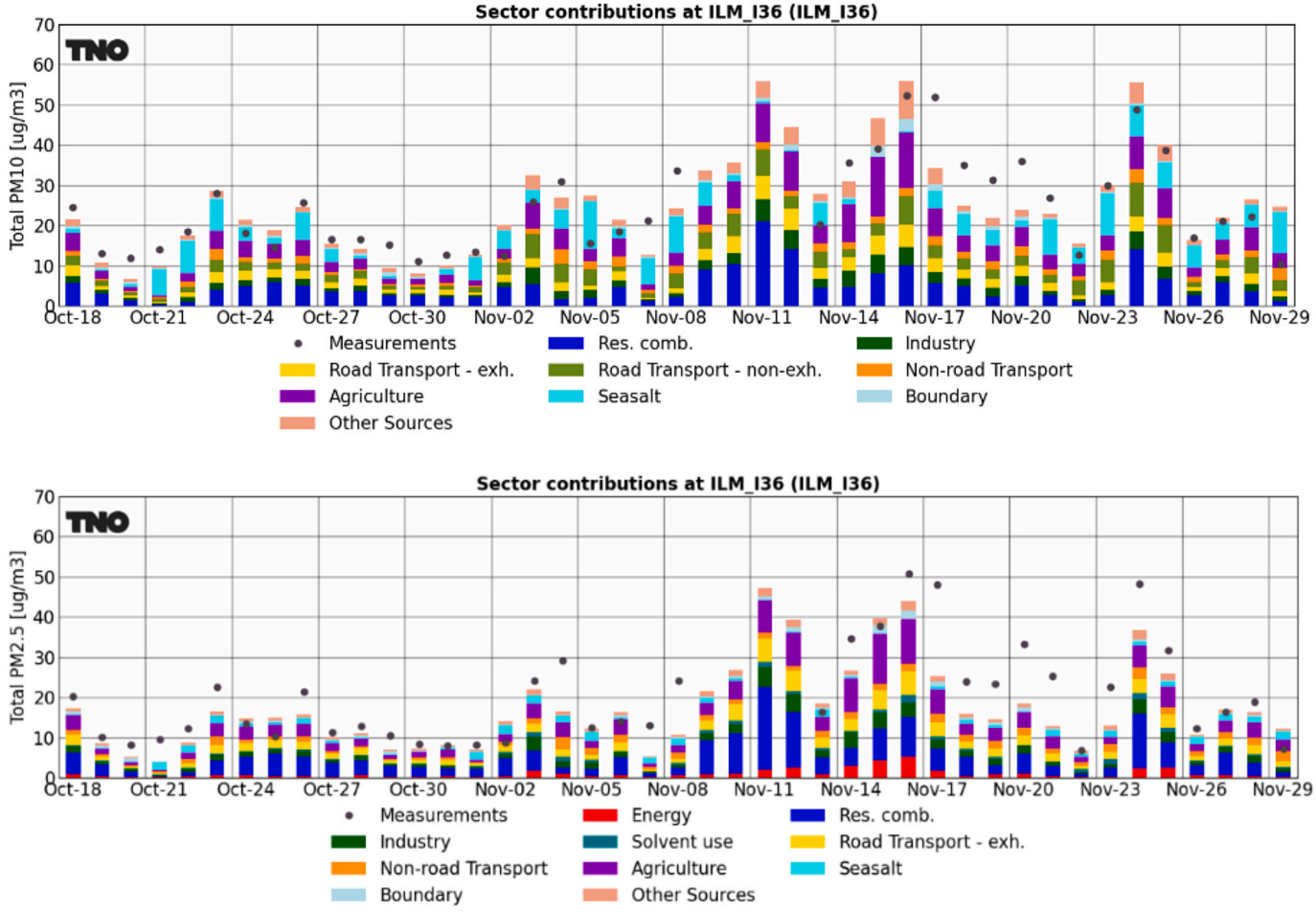

Fig. 16. PM_{10} (top) and $PM_{2.5}$ (bottom) sector contributed concentrations from TOPAS product between mid-October and November 2021 in the center of Eindhoven together with the corresponding measurements from ILM #36 station.

pm fine and pm coarse) and their precursors (NO_x, SO_x) to obtain PM simulations that better describe the measurements can be explained by the model's need to compensate for missing secondary organic aerosols.

The temporal profiles of the updated emissions in November 2021 over a grid cell located in the city center of Eindhoven have been compared with the *a priori* profiles. The average of the emissions per day-of-week normalized to the day-average of the week are calculated in order to compare the *a priori* with the updated weekly profiles. Fig. 17 shows these normalized values of PM fine (left) and PM coarse (right) emissions per day of the week for the *a priori*-inventory and the

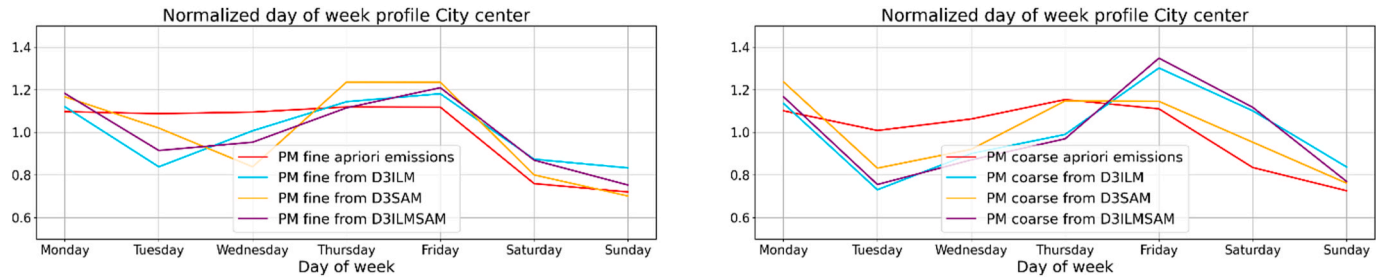

Fig. 17. Day-of-the-week profiles for the PM fine (left) and PM coarse (right) emissions for city center pixel normalized to day-average for the week.

estimated by the assimilations. Both PM fine and PM coarse emissions estimated with the "D3ILM" assimilation show an abrupt decline on Tuesday that is only slightly seen in PM coarse *a priori* profiles, while a peak is found on Friday which is most prominent in the PM coarse component. The "D3SAM" and "D3ILMSAM" emission profiles show as well a similar decline on Tuesday for the PM coarse component. The PM fine emissions from the "D3SAM" assimilation show a decrease on Wednesday which is not found in the experiments. In general the assimilations seem to suggest that *a priori* emissions should be decreased early in the week, but increased by the end of week and the weekend. We should note here that these results are based on few samples since this study covers a short time-period of a month. It is essential to study a longer period to extract more accurate results on temporal profiles.

Similar profiles for emissions as function of hour-of-the-day for the same city center cell are shown in Fig. 18. The profile of both PM fine and PM coarse emissions after assimilation follow quite well the profile of the *a priori* emissions during the early hours of the day (1 a.m.–6 a.m.). However, the *a posteriori* profile of the "D3ILM" assimilation shows a shorter (in duration) morning peak in both PM fine and PM coarse emissions compared to the *a priori*. The afternoon peak shown in the *a priori* profile around 16p.m. and 17p.m. is not present in any of the assimilation experiments, while a new peak is found between 11a.m. and 15p.m. During nighttime the *a priori* and *a posteriori* profiles agree quite well.

The fact that the two assimilation runs "D3ILM" and "D3SAM", that rely on observations of two independent networks, both suggest similar changes in day-of-week and hour-of-day profiles prompts to the importance of further research over longer time periods to find whether these changes are persistent and if specific source sectors require updates of their *a priori* profiles.

5. Conclusions and discussion

In this study we presented a methodology for integrating particulate matter measurements from heterogenous in situ networks and the LOTOS-EUROS CTM through a data assimilation technique. The experiments focus on a domain of about 0.5 km × 1 km resolution around the city of Eindhoven in the Netherlands. In this domain, two low-cost sensor networks observing particulate matter concentrations are available: ILM network and the SamenMeten citizen science network. In addition, a limited number of observations from the national official air quality monitoring network is available. Simulations for the target domain are nested into a wider domain in which additional stations from the official network are available too. The final results were obtained from 5 experiments that differ in the type of measurements that are assimilated and whether boundary conditions are incorporated from the wider domains from a standard model run or an assimilation of observations from the official network.

The results shown in this work indicate that simulations of PM concentrations over Eindhoven strongly improve when boundary conditions from an assimilation on the wider domain are used, and improved even further when measurements from low-cost sensors are assimilated too. A large underestimation of the measurements in the free run is strongly decreased in all different experiments that assimilate observations. For locations in the center of Eindhoven, the mean bias of PM_{10} ($PM_{2.5}$) in the free model run is equal to −36% (−56%) and reduces to −20% (−43%) when using boundary conditions from an assimilation. These results suggest that, for the chosen simulation period and the model setup, about 45% (23%) of the initial PM_{10} ($PM_{2.5}$) bias in the free model run is due to missing concentrations from outside the domain. Mean relative biases of PM_{10} in the city of Eindhoven drop to +6%, −1% and +6% when improved boundary conditions are used together with assimilation from the ILM, SamenMeten, or both networks together respectively. The correlation coefficient is improved from 0.75 in the free model run to a range between 0.87 and 0.91 depending on the assimilated sensors. Finally, the NRMSE decreases on average with about 0.25 compared to 0.47 in the free model run. In the only available official station near the city measuring $PM_{2.5}$ the assimilations including ILM data decrease the bias with about −27% compared to about −56% in the free model run and −43% for the free model run using assimilated boundary conditions.

The assimilation system was configured to estimate emission changes that lead to smaller difference between observations and simulations and to subsequently update the default temporal profiles of emissions which form one of the main sources of uncertainty in the model. The day-of-the-week and hour-of-the-day emission profiles derived from the assimilation of low-cost sensors suggest differences compared to the *a priori* profiles used. An abrupt decline in emissions on Tuesday and on Wednesday is suggested from the assimilations of ILM and SamenMeten data. In the hour-of-the-day profiles the assimilations

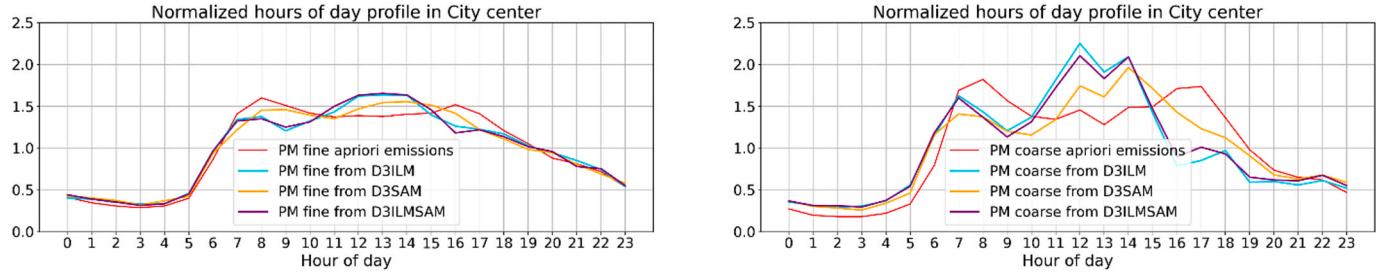

Fig. 18. Normalized hourly profiles for the PM fine (left) and PM coarse (right) emissions for city center pixel.

suggest an afternoon peak in PM fine and PM coarse between 11a.m. and 14p.m., while this peak is shown later (between 15p.m. and 18p.m.) in *a priori* profiles.

Despite the uncertainties and limitations that characterize the SamenMeten citizen science network, the experiments show that it is feasible to exploit the dataset and extract useful information. Assimilation of these observations lead to similar adjustments of concentrations as seen for assimilation of the low-cost sensor data from the ILM network. The result supports the idea of monitoring urban air quality using additional networks next to the official measurement stations.

When evaluated of a longer time period, the assimilation results could point to adjustments or uncertainties in the prior emissions inventories that are used to adjust concentrations. It should however kept in mind that the uncertainties currently assigned to emissions probably also account for other model uncertainties. In this context the experiments shown for example the high importance of the boundary conditions in the studied region.

Future work should focus on a more detailed study of the emission correction factors extracted from this method in order investigate which emission sources are in particular uncertain and might be underestimated in the region. Temporal profiles of PM emissions need also further investigation since both independent experimental runs (using ILM or SamenMeten sensors) suggest similar changes in *a priori* profiles. Secondary organic aerosols should be prioritized in model implementations since their contribution in total PM is important, and is highly advised to include this in similar studies. Finally, the parameterization of emission and other model uncertainties in terms of their amplitude and spatial and temporal correlation scales requires permanent attention and improvement.

CRediT authorship contribution statement

Ioanna Skoulidou: Writing – original draft, Visualization, Validation, Software, Methodology, Data curation. **Arjo Segers:** Writing – review & editing, Supervision, Methodology. **Bas Henzing:** Writing – review & editing, Supervision, Methodology, Funding acquisition, Conceptualization. **Jun Zhang:** Writing – review & editing, Data curation. **Ruben Goudriaan:** Writing – review & editing, Supervision, Project administration, Conceptualization. **Maria-Elissavet Koukouli:** Writing – review & editing, Supervision. **Dimitrios Balis:** Writing – review & editing, Supervision.

Declaration of competing interest

The authors declare that they have no known competing financial interests or personal relationships that could have appeared to influence the work reported in this paper.

Data availability

Data will be made available on request.

Acknowledgments

The research was part of the TNO research program Exposense

Appendix A. Supplementary data

Supplementary data to this article can be found online at https://doi.org/10.1016/j.atmosenv.2024.120652.

References

Ascenso, A., Augusto, B., Silveira, C., Rafael, S., Coelho, S., Monteiro, A., Ferreira, J., Menezes, I., Roebeling, P., Miranda, A.I., 2021. Impacts of nature-based solutions on the urban atmospheric environment: a case study for Eindhoven, The Netherlands. Urban For. Urban Green. 57, 126870 https://doi.org/10.1016/j.ufug.2020.126870.

Blocken, B., Vervoort, R., van Hooff, T., 2016. Reduction of outdoor particulate matter concentrations by local removal in semi-enclosed parking garages: a preliminary case study for Eindhoven city center. J. Wind Eng. Ind. Aerod. 159, 80–98. https://doi.org/10.1016/j.jweia.2016.10.008.

Canu, M., Gálvis, B., Madelin, M., 2021. What does the Shinyei PPD42NS low-cost dust sensor really measure? Int. J. Environ. Sustain Dev. 12 (1), 1–9. https://doi.org/10.18178/ijesd.2021.12.1.1310.

Castellanos, P., Boersma, K.F., 2012. Reductions in nitrogen oxides over Europe driven by environmental policy and economic recession. Sci. Rep. 2 (1), 1–7. https://doi.org/10.1038/srep00265.

CBS, 2019. Centraal Bureau voor de Statistiek. https://www.cbs.nl/.

Curier, R.L., Timmermans, R., Calabretta-Jongen, S., Eskes, H., Segers, A., Swart, D., Schaap, M., 2012. Improving ozone forecasts over Europe by synergistic use of the LOTOS-EUROS chemical transport model and in-situ measurements. Atmos. Environ. 60, 217–226. https://doi.org/10.1016/j.atmosenv.2012.06.017.

EEA, 2019. EMEP/EEA Air Pollutant Emission Inventory Guidebook. https://www.eea.europa.eu/publications/emep-eea-guidebook-2019. (Accessed 4 April 2022).

Fioletov, V., McLinden, C., Griffin, D., Krotkov, N., Liu, F., Eskes, H., 2021. Quantifying urban, industrial, and background changes in NO_2 during the COVID-19 lockdown period based on TROPOMI satellite observations. Atmos. Chem. Phys. 1–48. https://doi.org/10.5194/acp-2021-536.

Forster, P., Ramaswamy, V., Artaxo, P., Berntsen, T., Betts, R., Fahey, D.W., Haywood, J., Lean, J., Lowe, D.C., Myhre, G., 2007. Chapter 2. Changes in atmospheric constituents and in radiative forcing. Clim. Change 2007. Phys. Sci. 20 (7), 129–234.

Fountoukis, C., Nenes, A., 2007. ISORROPIA II: a computationally efficient thermodynamic equilibrium model for for K+–Ca2+–Mg2+–NH4+–Na+–SO42−–NO3−–Cl−–H2O aerosols. Atmos. Chem. Phys 7, 4639–4659. https://doi.org/10.5194/acp-7-4639-2007.

Gašparac, G., Jeričević, A., Kumar, P., Grisogono, B., 2020. Regional-scale modelling for the assessment of atmospheric particulate matter concentrations at rural background locations in Europe. Atmos. Chem. Phys. 20 (11), 6395–6415. https://doi.org/10.5194/acp-20-6395-2020.

Gery, M.W., Whitten, G.Z., Killus, J.P., Dodge, M.C., 1989. A photochemical kinetics mechanism for urban and regional scale computer modeling. J. Geophys. Res. 94 (D10), 12925–12956. https://doi.org/10.1029/jd094id10p12925.

Goudriaan, R., Zhang, J., Tokaya, J., Hensen, A., van Dinther, D., Kaandorp, S., Blom, M., Plomp, A., 2022. Regionaal Meetnet ILM2 in Zuidoost-Brabant: Jaarrapportage 2021. https://samenmeten.nl/sites/default/files/2023-01/R12396_ILM2_Jaarrapport2021-technischjaarverslagmeetnetZOB.pdf.

Hama, S., Ouchen, I., Wyche, K.P., Cordell, R.L., Monks, P.S., 2022. Carbonaceous aerosols in five European cities: insights into primary emissions and secondary particle formation. Atmos. Res. 274, 106180 https://doi.org/10.1016/j.atmosres.2022.106180.

Hamm, N.A.S., van Lochem, M., Hoek, G., Otjes, R., van der Sterren, S., Verhoeven, H., 2016. "The invisible made visible": science and technology. AiREAS: Sustainocracy for a Healthy City 51–77. https://doi.org/10.1007/978-3-319-26940-5_3.

Hunt, B.R., Kostelich, E.J., Szunyogh, I., 2007. Efficient data assimilation for spatiotemporal chaos: a local ensemble transform Kalman filter. Phys. Nonlinear Phenom. 230 (1–2), 112–126.

Kaiser, J.W., Heil, A., Andreae, M.O., Benedetti, A., Chubarova, N., Jones, L., Morcrette, J.J., Razinger, M., Schultz, M.G., Suttie, M., Van Der Werf, G.R., 2012. Biomass burning emissions estimated with a global fire assimilation system based on observed fire radiative power. Biogeosciences 9 (1), 527–554. https://doi.org/10.5194/bg-9-527-2012.

Kampa, M., Castanas, E., 2008. Human health effects of air pollution. Environ. Pollut. 151 (2), 362–367. https://doi.org/10.1016/j.envpol.2007.06.012.

Karagulian, F., Belis, C.A., Dora, C.F.C., Prüss-Ustün, A.M., Bonjour, S., Adair-Rohani, H., Amann, M., 2015. Contributions to cities' ambient particulate matter (PM): a systematic review of local source contributions at global level. Atmos. Environ. 120, 475–483. https://doi.org/10.1016/j.atmosenv.2015.08.087.

Kuenen, J., Dellaert, S., Visschedijk, A., Jalkanen, J.-P., Super, I., van der Gon, H., 2022. CAMS-REG-v4: a state-of-the-art high-resolution European emission inventory for air quality modelling. Earth Syst. Sci. Data 14 (2), 491–515.

Kuenen, J.J.P., Visschedijk, A.J.H., Jozwicka, M., Denier Van Der Gon, H.A.C., 2014. TNO-MACC-II emission inventory; A multi-year (2003-2009) consistent high-resolution European emission inventory for air quality modelling. Atmos. Chem. Phys. 14 (20), 10963–10976. https://doi.org/10.5194/acp-14-10963-2014.

Liu, H.Y., Dunea, D., Iordache, S., Pohoata, A., 2018. A review of airborne particulate matter effects on young children's respiratory symptoms and diseases. Atmosphere 9 (4), 150. https://doi.org/10.3390/atmos9040150.

Lopes, D., Ferreira, J., Hoi, K.I., Yuen, K.V., Mok, K.M., Miranda, A.I., 2021. Emission inventories and particulate matter air quality modeling over the pearl river delta region. Int. J. Environ. Res. Publ. Health 18 (8), 4155. https://doi.org/10.3390/ijerph18084155.

Lopez-Restrepo, S., Yarce, A., Pinel, N., Quintero, O.L., Segers, A., Heemink, A.W., 2020. Forecasting PM10 and PM2.5 in the aburrá valley (Medellín, Colombia) via EnKF based data assimilation. Atmos. Environ. 232, 117507 https://doi.org/10.1016/j.atmosenv.2020.117507.

Lopez-Restrepo, S., Yarce, A., Pinel, N., Quintero, O.L., Segers, A., Heemink, A.W., 2021. Urban air quality modeling using low-cost sensor network and data assimilation in the aburrá valley, Colombia. Atmosphere 12 (1), 91. https://doi.org/10.3390/ATMOS12010091.

Manders, A.M.M., Builtjes, P.J.H., Curier, L., Gon, H.A.C.D. Vander, Hendriks, C., Jonkers, S., Kranenburg, R., Kuenen, J.J.P., Segers, A.J., Timmermans, R.M.A., Visschedijk, A.J.H., Kruit, R.J.W., Pul, W.A.J.V., Sauter, F.J., Van Der Swaluw, E., Swart, D.P.J., Douros, J., Eskes, H., Van Meijgaard, E., Schaap, M., 2017. Curriculum

vitae of the LOTOS-EUROS (v2.0) chemistry transport model. Geoscientific Model Development 10 (11), 4145–4173. https://doi.org/10.5194/gmd-10-4145-2017.
Mårtensson, E.M., Nilsson, E.D., de Leeuw, G., Cohen, L.H., Hansson, H.-C., 2004. Laboratory simulations and parameterization of the primary marine aerosol production. J. Geophys. Res.: Atmosph. 108 (D9) https://doi.org/10.1029/2002JD002263.
Mijling, B., 2020. High-resolution mapping of urban air quality with heterogeneous observations: a new methodology and its application to Amsterdam. Atmos. Meas. Tech. 13 (8), 4601–4617. https://doi.org/10.5194/amt-13-4601-2020.
Mijling, B., Jiang, Q., De Jonge, D., Bocconi, S., 2018. Field calibration of electrochemical NO2 sensors in a citizen science context. Atmos. Meas. Tech. 11 (3), 1297–1312. https://doi.org/10.5194/amt-11-1297-2018.
Monahan, E.C., Spiel, D.E., Davidson, K.L. (Eds.), 1986. A model of marine aerosol generation via whitecaps and wave disruption, in Oceanic Whitecaps. Springer, Netherlands, pp. 167–174.
Novak, J.H., Pierce, T.E., 1993. Natural emissions of oxidant precursors. Water, Air, & Soil Pollution 67 (1–2), 57–77. https://doi.org/10.1007/BF00480814.
Paulot, F., Jacob, D.J., Pinder, R.W., Bash, J.O., Travis, K., Henze, D.K., 2014. Ammonia emissions in the United States, European Union, and China derived by high-resolution inversion of ammonium wet deposition data: interpretation with a new agricultural emissions inventory (MASAGE_NH3). J. Geophys. Res. 119 (7), 4343–4364. https://doi.org/10.1002/2013JD021130.
Popoola, O.A.M., Carruthers, D., Lad, C., Bright, V.B., Mead, M.I., Stettler, M.E.J., Saffell, J.R., Jones, R.L., 2018. Use of networks of low cost air quality sensors to quantify air quality in urban settings. Atmos. Environ. 194, 58–70. https://doi.org/10.1016/j.atmosenv.2018.09.030.
Rubio-Iglesias, J.M., Edovald, T., Grew, R., Kark, T., Kideys, A.E., Peltola, T., Volten, H., 2020. Citizen science and environmental protection agencies: engaging citizens to address key environmental challenges. Front. Clim. 2, 24. https://doi.org/10.3389/fclim.2020.600998.
Saikawa, E., Kurokawa, J., Takigawa, M., Borken-Kleefeld, J., Mauzerall, D.L., Horowitz, L.W., Ohara, T., 2011. The impact of China's vehicle emissions on regional air quality in 2000 and 2020: a scenario analysis. Atmos. Chem. Phys. 11 (18), 9465–9484. https://doi.org/10.5194/acp-11-9465-2011.
Schaap, M., Manders, A.M.M., Hendriks, C., Cnossen, J.M., Segers, A.J., Denier van der Gon, H., Jozwicka, M., Sauter, F.J., Velders, G.J.M., Matthijsen, J., Builtjes, P.J.H., 2009. *Regional Modelling of Particulate Matter for the Netherlands*.
Schneider, P., Castell, N., Vogt, M., Dauge, F.R., Lahoz, W.A., Bartonova, A., 2017. Mapping urban air quality in near real-time using observations from low-cost sensors and model information. Environ. Int. 106, 234–247. https://doi.org/10.1016/j.envint.2017.05.005.
Shin, S., Kang, J.S., Jo, Y., 2016. The local ensemble transform kalman filter (LETKF) with a global NWP model on the cubed sphere. Pure Appl. Geophys. 173 (7), 2555–2570. https://doi.org/10.1007/s00024-016-1269-0.
Skoulidou, I., Koukouli, M.E., Segers, A., Manders, A., Balis, D., Stavrakou, T., van Geffen, J., Eskes, H., 2021. Changes in power plant nox emissions over northwest Greece using a data assimilation technique. Atmosphere 12 (7). https://doi.org/10.3390/atmos12070900.
Solazzo, E., Galmarini, S., Bianconi, R., Rao, T., 2013. Model evaluation for surface concentration of particulate matter in Europe and north America in the context of AQMEII. NATO Sci. Peace Sec. C: Environ. Secur. 137, 375–379. https://doi.org/10.1007/978-94-007-5577-2_63.
Timmermans, R., van Pinxteren, D., Kranenburg, R., Hendriks, C., Wadinga Fomba, K., Schaap, M., 2022. Evaluation of modelled lotos-euros with observational based Pm10 source attribution. SSRN. https://doi.org/10.2139/ssrn.4025844.
Viatte, C., Wang, T., Van Damme, M., Dammers, E., Meleux, F., Clarisse, L., Shephard, M. W., Whitburn, S., François Coheur, P., Cady-Pereira, K.E., Clerbaux, C., 2020. Atmospheric ammonia variability and link with particulate matter formation: a case study over the Paris area. Atmos. Chem. Phys. 20 (1), 577–596. https://doi.org/10.5194/acp-20-577-2020.
Wang, Z., Pan, L., Li, Y., Zhang, D., Ma, J., Sun, F., Xu, W., Wang, X., 2015. Assessment of air quality benefits from the national pollution control policy of thermal power plants in China: a numerical simulation. Atmos. Environ. 106, 288–304. https://doi.org/10.1016/j.atmosenv.2015.01.022.
Wesseling, J., de Ruiter, H., Blokhuis, C., Drukker, D., Weijers, E., Volten, H., Vonk, J., Gast, L., Voogt, M., Zandveld, P., van Ratingen, S., Tielemans, E., 2019. Development and implementation of a platform for public information on air quality, sensor measurements, and citizen science. Atmosphere 10 (8), 445. https://doi.org/10.3390/atmos10080445.
WHO, 2021. Ambient (outdoor) air pollution fact sheets. https://www.who.int/news-room/fact-sheets/detail/ambient-(outdoor)-air-quality-and-health. (Accessed 3 November 2023).
Zhao, B., Wang, S., Dong, X., Wang, J., Duan, L., Fu, X., Hao, J., Fu, J., 2013. Environmental effects of the recent emission changes in China: implications for particulate matter pollution and soil acidification. Environ. Res. Lett. 8 (2), 24031 https://doi.org/10.1088/1748-9326/8/2/024031.